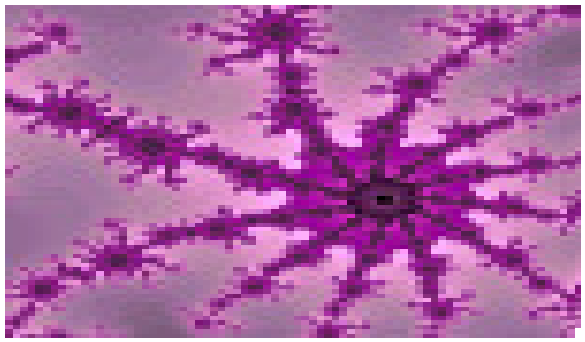

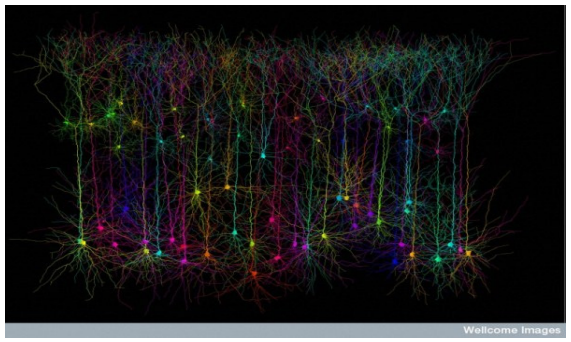

La complessità della realtà biologica interpretata tramite la geometria frattale

Gabriele A. Losa Prof. PhD
European Academy of Sciences
Chairman Fractals in Biology and Medicine
Institute of Scientific Interdisciplinary Studies [ISSI]
Locarno Switzerland
e-mail: glosa@cerfim.ch

POLITECNICO DI MILANO

Anno accademico 2013/2014 6° ciclo di seminari FDS
Aula Consiglio del Dipartimento di Matematica
4 dicembre 2013 ore 15.00

Le forme biologiche

Stato attuale: il problema della forma costituisce il nocciolo centrale nella comprensione ed elucidazione dei processi biologici e genetici .

- La biologia risulta dall'interazione (interplay) fra:
  caso (hasard, randomness): ruolo nell'evoluzione
  non linearità (nonlinearity): creazione delle forme
  complessità (complexité, complexity): generazione, modellatura (adattamento) (modelage, adaptation) delle forme .
- Studio delle forme biologiche:
- **Leonardo da Vinci** : « Nessuna humana investigatione si può dimandare vera scienza s'essa non passa per le matematiche dimostrazioni >. (MSA 100): …. la natura,…. la quale con filosofia e sottile speculazione considera tutte le qualità delle forme, …e siti, piante, animali, erbe e fiori, le quali sono cinte d'ombra e di luce. E veramente questa è scienza ….
- **Galileo Galilei** : « l'Universo è scritto in lingua matematica, e i caratteri son triangoli, cerchi ed altre figure geometriche.. «
- **D'Arcy Thompson**: « En général les formes n'existent pas, sauf celles qui sont conformes aux lois de la physique et de la mathématique.
- **E. Kant** : E. Kant : The organization of forms is an abyss impenetrable to the mind.
- Ma quale linguaggio ?
  Convenzionale, matematico analitico, geometria frattale, altro ?

Mandelbrot : ‘‘. . clouds are not spheres, mountains are not cones, coastlines are not circles, and bark is not smooth, nor does lightning travel in a stright line ‘‘.

The Irruption of Fractal Geometry in Biology and Medicine

- Although there is no precise date, it is generally agreed that the introduction of Fractal Geometry into the life sciences, such as biology and medicine, occurred within the ‘‘golden age’’ of cell biology – that is, between the 1960s and 1990s.
- There was a striking debate within the biologist community, about the morphofunctional complexity of cells and tissues and how to measure it.
- The discovery that cellular membrane systems have fractal properties arose from the uncertainty of observations regarding the extent of such membranes. When the results of the first studies on the morphometry of liver cell membranes were reported, the values obtained were much higher than had been reported by others; in fact liver cells were found to contain *6 or 11m^2 of membranes per cm^3* . Which one of these estimates was correct ?
- The systematic measurement of irregular liver cell membranes revealed that the estimates of surface density increased with increased resolution [Paumgartner et al.]. Shortly after the conclusion of the experimental study, Mandelbrot suggested that the results should be interpreted with the likely effect of the ‘‘*resolution scale*,’’ in analogy with the ‘‘Coast of Britain effect’’ . (Not Euclidean linear bodies).

Paumgartner, D., Losa, G.A., Weibel, E.R. (1981). Resolution effect on the stereological estimation of surface and volume and its interpretation in terms of fractal dimensions. *J. Microsc.* **121**, 51–63.
Mandelbrot, B. (1967) How long is the coast of Britain? Statistical self-similarity and fractional dimension. *Science* **155**,636–640.

Scale length effect

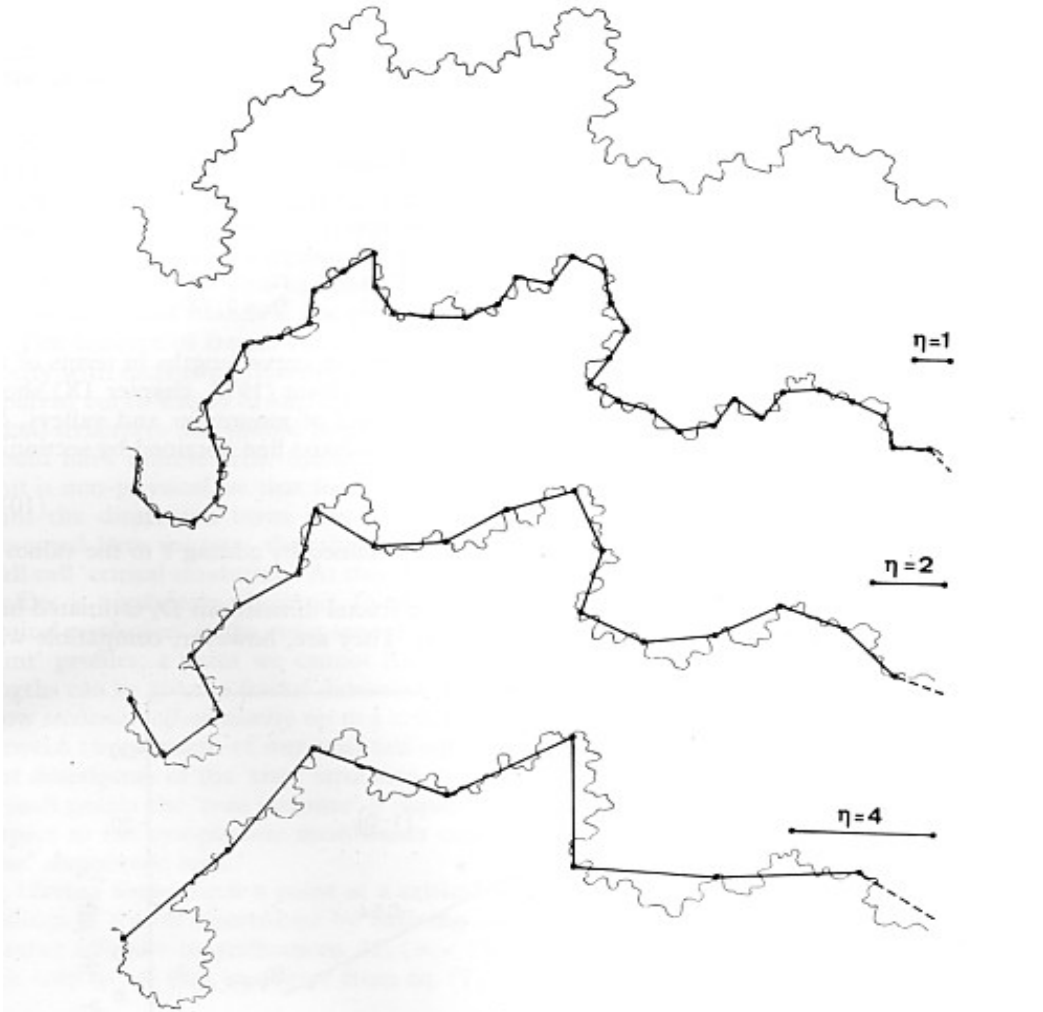

Fig. 8. Approximate estimation of length of curve by fitting polygon of varying 'scale' length η.

Main Properties of Fractal Elements

- Self-similarity [geometrical or statistical]
- Form invariance by scaling
- Shape irregularity (rugosity)
- Iteration of the generator
- Fractal dimension FD (fractional/non-integer)
- Mandelbrot-Richardson equation: scaling power law

$$\log \frac{L(\varepsilon)}{lo} = (1-D) \log \frac{(\varepsilon)}{lo}$$

Remark: The complexity and the self-similarity of biological shapes are constructed from inherent simplicity (uncomplicated rules), i.e. by the iteration of an invariant simple pattern that spans several length scales.

Fractal Geometry

Unifying description of not uniform natural phenomena and structures

Mathematical fractals

exact self-similar, invariant over an unlimited range of scales (ε)

Biological (natural) fractals

- statistically self-similar
- invariant within a finite range of ε values - **scaling window** - defined by upper and lower limits (ε_1: ε_2) on a log-log plot spreading at least two orders of magnitude.
- measured properties (functional/ morphological/ temporal) depend on scaling (i.e. on magnification / scale of observation)
- high level of organization (complexity)

Mathematical basis

Mandelbrot-Richardson equation $L(\varepsilon) = N(\varepsilon).(\varepsilon)$

and $N(\varepsilon) = l_0^D \varepsilon^{-D}$

Dimensionless Scaling Power Law $\frac{L(\varepsilon)}{lo} = \left[\frac{\varepsilon}{[lo]}\right]^{1-D}$

The logarithmic transformation yields a straight line equation

$$\log \frac{L(\varepsilon)}{lo} = (1-D) \log \frac{(\varepsilon)}{lo}$$

Fractal dimension [D]: estimated from the slope (1-D) of the straight line drawn on a log-log plot

The fractality of natural objects

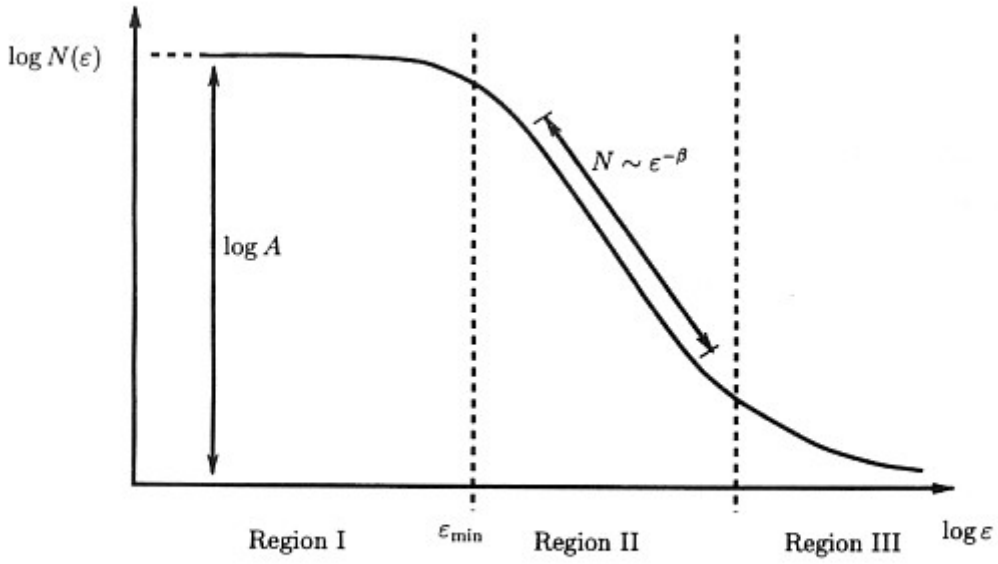

Figure 1. The three typical regions of an asymptotic fractal. Typically, natural fractals are limited by a lower and an upper bound and only show fractality in region II, as indicated by the straight line.

The Scaling Window

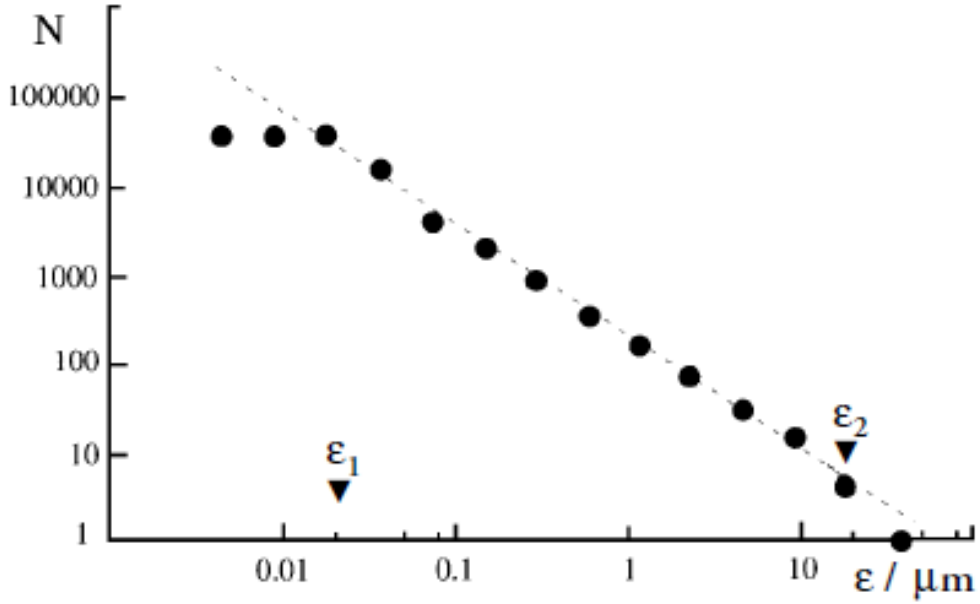

- A typical N versus **ε** plot (log-log scale) based on the power law $N(\varepsilon) = \varepsilon^{(1-D)}$
- ***The scaling window*** is clearly indicated: ε_1(0.025 mm) – ε_2 (25 mm).
- The slope of the straight line which could be plotted within this window is used to calculate the fractal dimension [D]. Box-counting method: the ordinate N (number of boxes) increases as the pixel length (**ε**) decreases, showing that the outline length of the object examined also increases within the scaling interval ε_1-ε_2.
  Ex.: NMBHC from MCF-7 breast cancer cells treated with 10^{-9} M estradiol.

FIGURE 4.1. *Schéma de deux lois théoriques pour la distribution des fréquences des mots.*

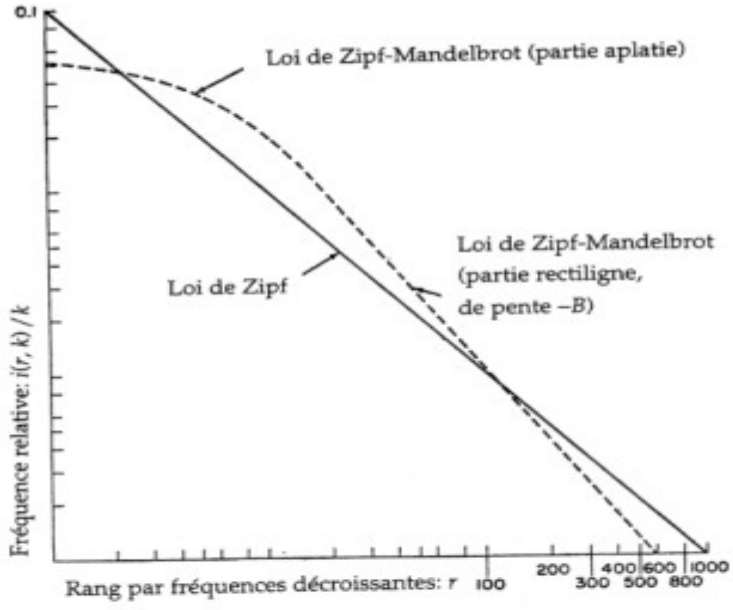

Mitochondria

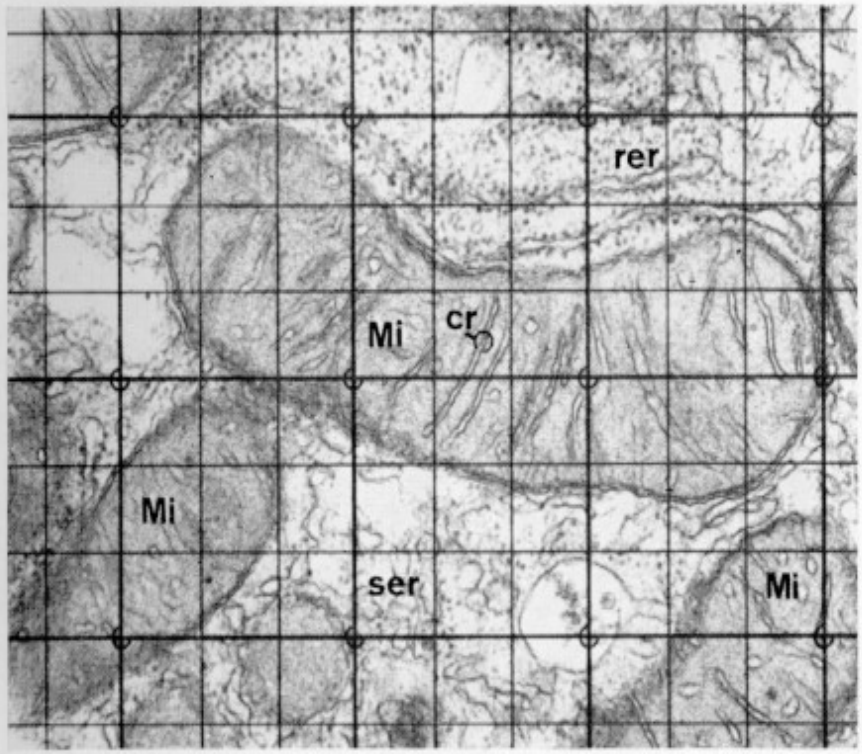

Figs. 1–4. Electron micrographs of hepatocyte cytoplasm with test systems superimposed as used for study. Mitochondria (Mi) show outer (omi) and inner (imi) membrane, and cristae (cr). Endoplasmic reticulum membranes occur in smooth (ser) and rough (rer) form due to ribosomes (rib) (see labels on Fig. 2). **Fig. 1.** Magnification × 38,000.

where λ and D are 'constants' which depend on the nature of the curve: Mandelbrot (1977) has shown that D can be interpreted as a dimension, whereas λ is the 'approximate measure of the curve in dimension D' and is independent of η. Introducing eq. (2) into eq. (1) we find that the estimated curve length is

$$B(\eta) = \lambda \cdot \eta^{1-D} \tag{3}$$

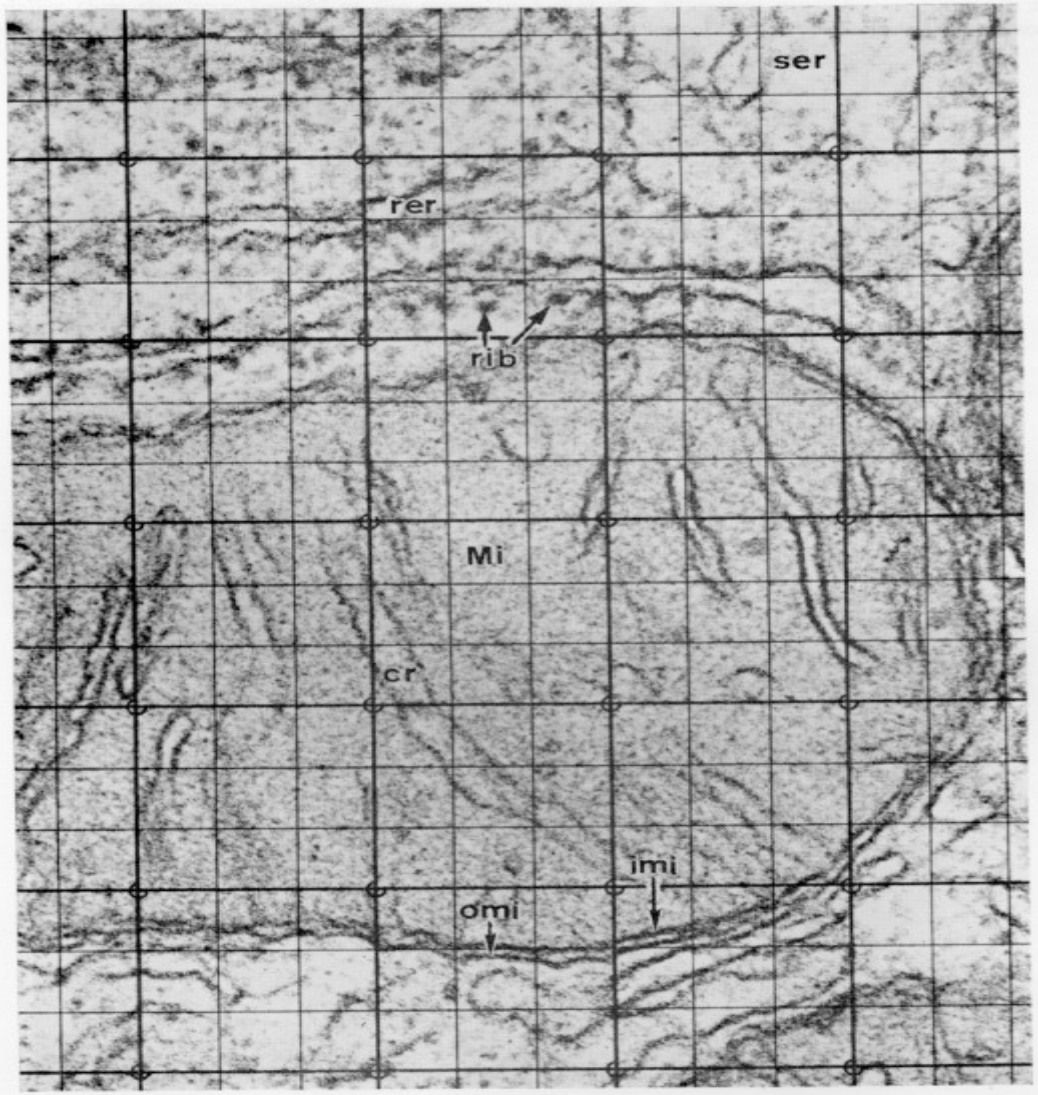

Fig. 4. Magnification $\times 130{,}000$.

Surface density estimates for outer and inner mitochondrial membranes

Paumgartner et al. J. Microscopy 1981;**121**:51

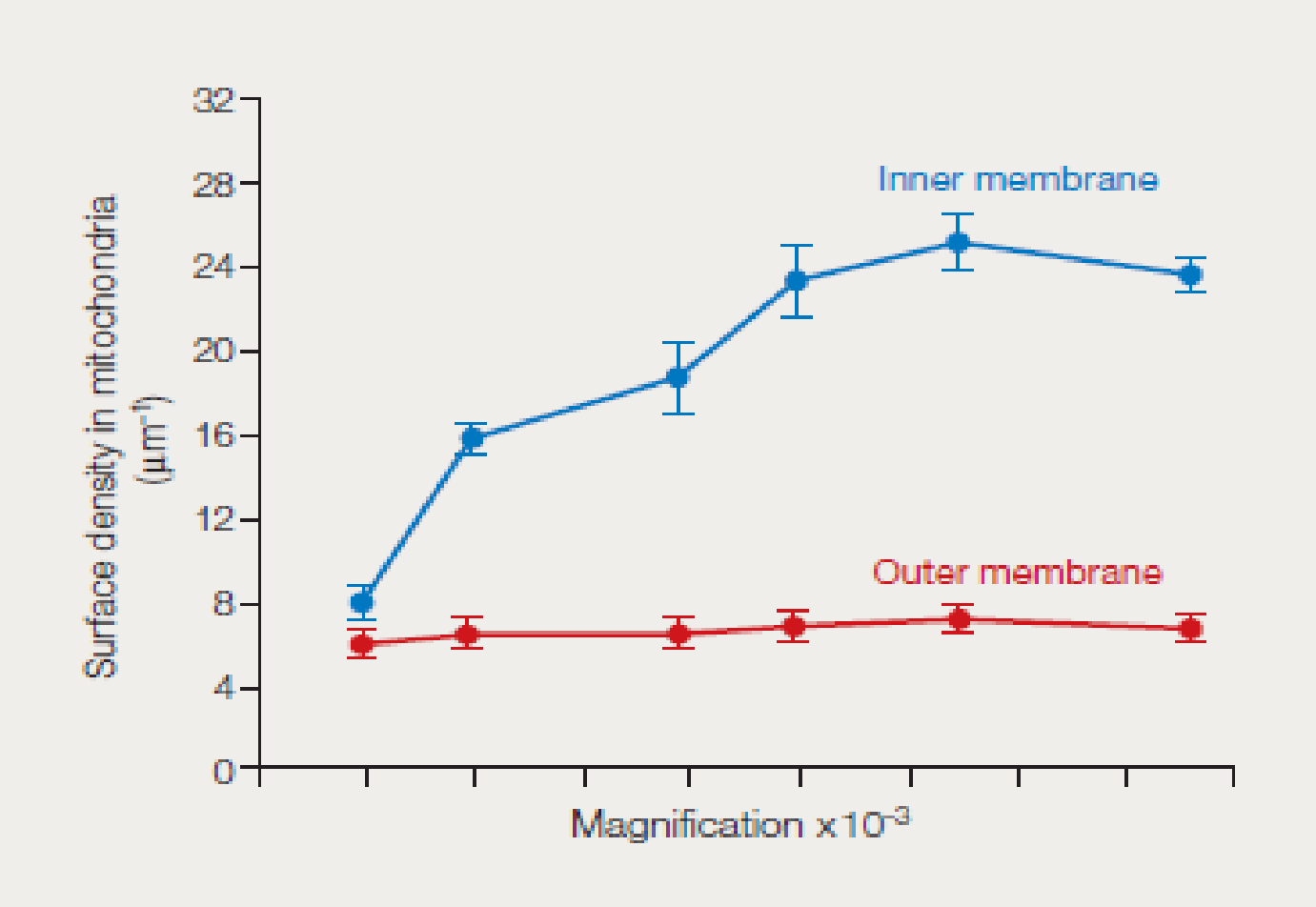

Resolution scale

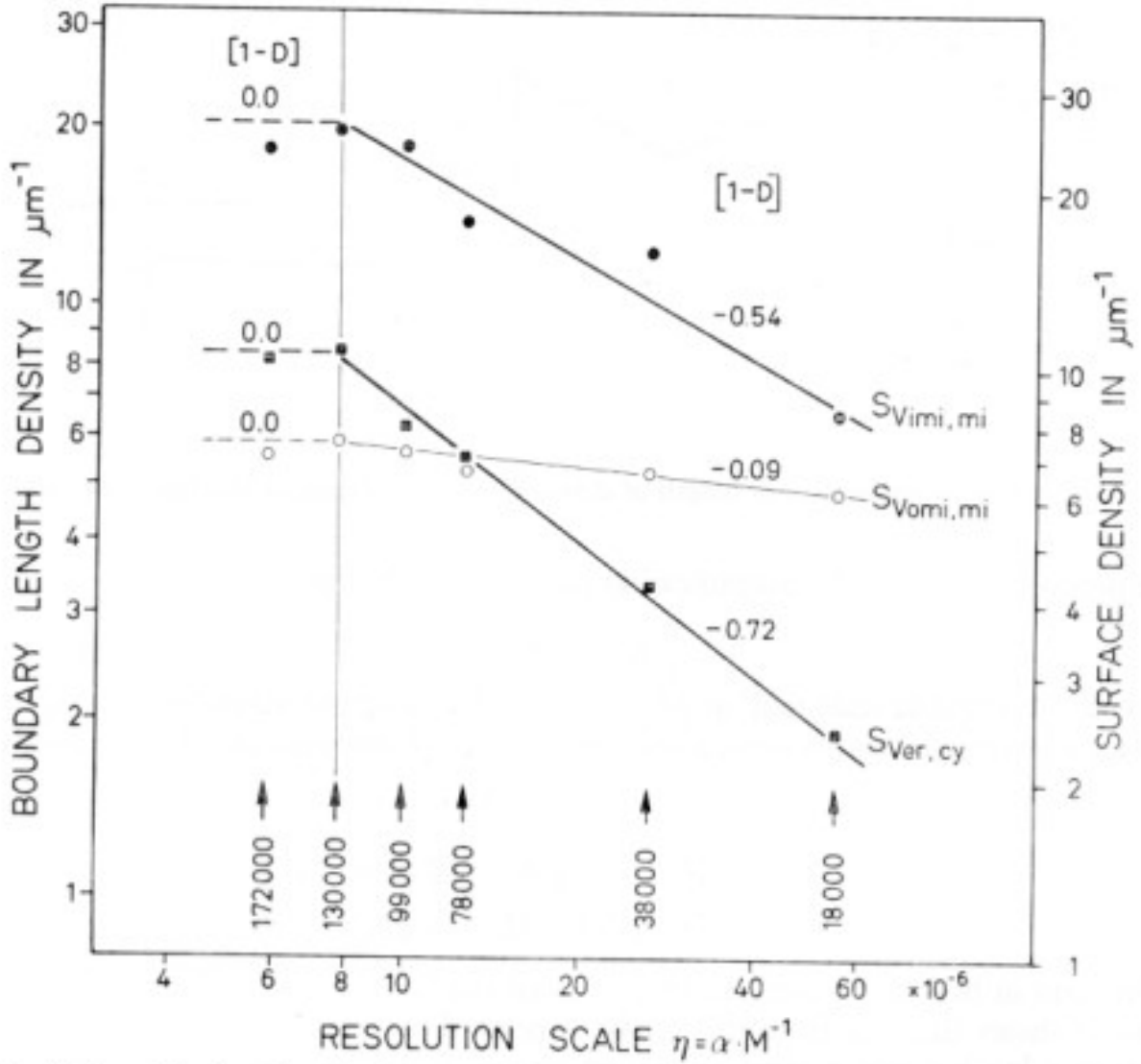

Fig. 9. Double-logarithmic plot of estimates of boundary length density against resolution scale (M^{-1}). Slope of regression line in the range $\{\times 18{,}000 < M < \times 130{,}000\}$ allows estimation of fractal dimension D. Note that $S_V = (4/\pi) \cdot B_A$.

Normal Breast Tissue / Invasive Carcinoma

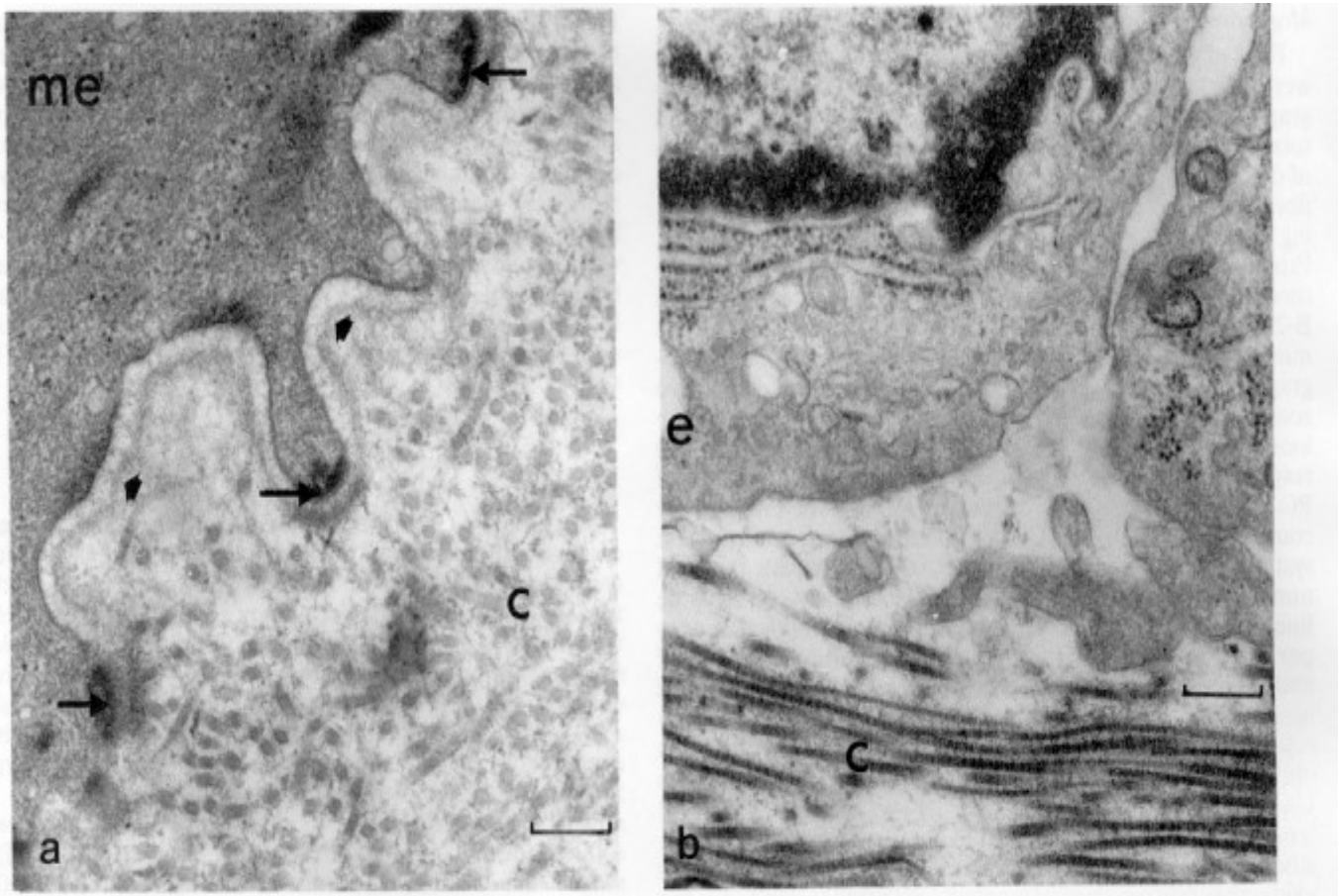

FIGURE 1 – *(a)* Normal breast tissue. EM view of myo-epithelial cell (me) attached to the lamina densa (◗) of the basement membrane by half desmosomes (→). C, collagen fibril. Magnification × 39100. Bar, 1 cm = 256 nm. *(b)* Invasive carcinoma of the breast. EM view of epithelial cells (e) adjacent to the dense connective tissue. The basement membrane is absent. Magnification × 39100. Bar, 1 cm = 256 nm.

CD-8 T-cell

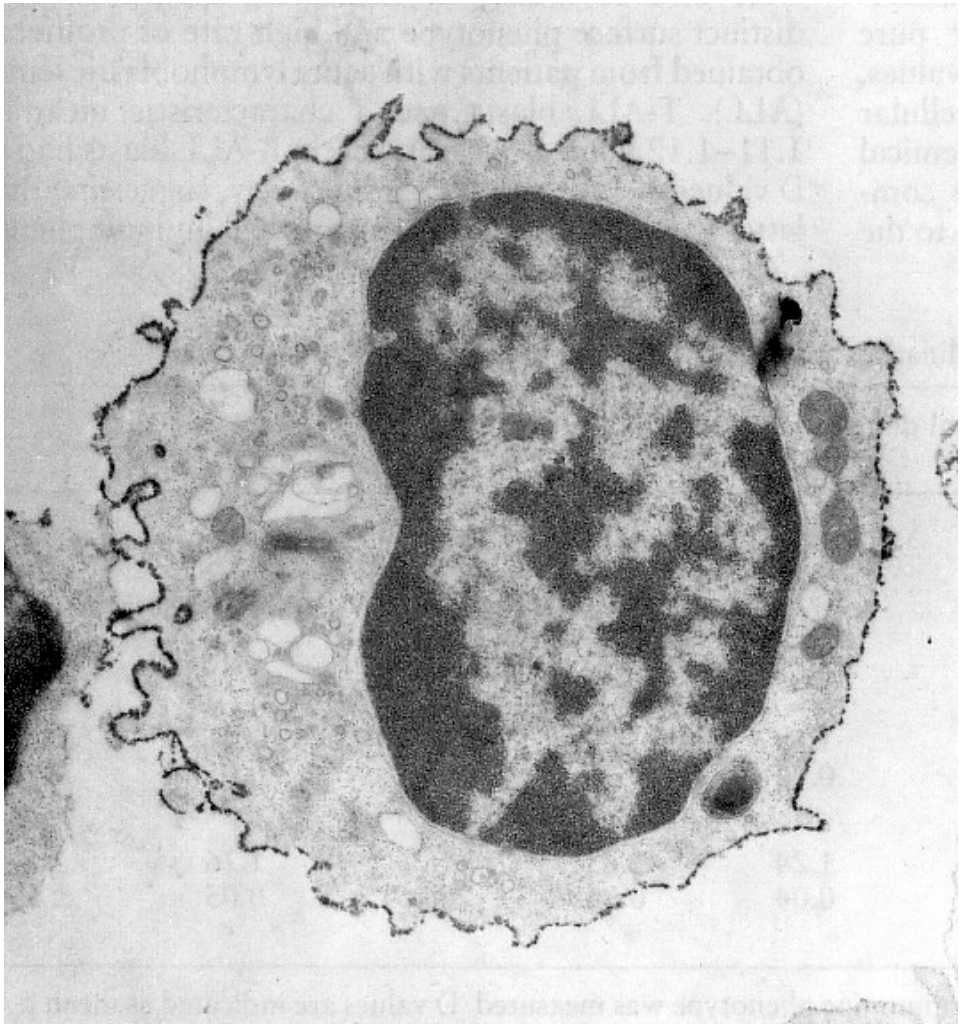

T-ALL

Fractal dimension of lymphocytes and leukemic cells

Table 1. Fractal dimensions (five moments) of pericellular membranes from resting and lectin activated lymphocytes

Cells	Fractal dimensions D 1	D 2	D 3	D 4	D 5	SD ±
T-lymphocytes (n.d)	1.19	1.20	1.21	1.21	1.22	0.04
T-lymphocytes (CD 8+)	1.22	1.23	1.23	1.23	1.23	0.04
T-lymphocytes (CD 4+)	1.17	1.16	1.16	1.16	1.17	0.04
PBMN (CD 3+)	1.20	1.20	1.20	1.20	1.21	0.05
PHA-stimulated PBMN (n.d.)	1.11	1.11	1.12	1.12	1.12	0.03

The profile of twenty elements for each cell population was measured. PHA: phytohemagglutinin. PBMN: human peripheral blood mononuclear cells. n.d.: not decorated with monoclonal antibodies. D values are given as the mean ± 1 SD. SD for D 1, D 2, D 3, D 4, D 5 were similar for a given cell population.

Table 2. Fractal dimensions (five moments) of pericellular membranes from lymphoblastic leukemia

Leukemia	Fractal dimensions D 1	D 2	D 3	D 4	D 5	SD ±
T-ALL (n.d.)	1.10	1.11	1.11	1.11	1.11	0.03
T-ALL (CD 2+)	1.12	1.12	1.12	1.12	1.12	0.02
B-ALL (early) (n.d.)	1.14	1.14	1.15	1.16	1.18	0.02
B-ALL (n.d.)	1.13	1.13	1.13	1.12	1.12	0.03
B-ALL (CD 19+)	1.19	1.19	1.19	1.19	1.19	0.03
HAIRY	1.32	1.33	1.34	1.35	1.36	0.03

ALL = Acute lymphoblastic leukemia with more than 95% of circulating blasts. Early B-ALL blasts were found Calla and CD 19 positive. B-ALL blasts were found Calla negative and CD 19, CD 20 positive. n.d.: not decorated with monoclonal antibodies unless indicated (CD+).

Steroid hormones on nuclear heterochromatin (MCF-7 cells)

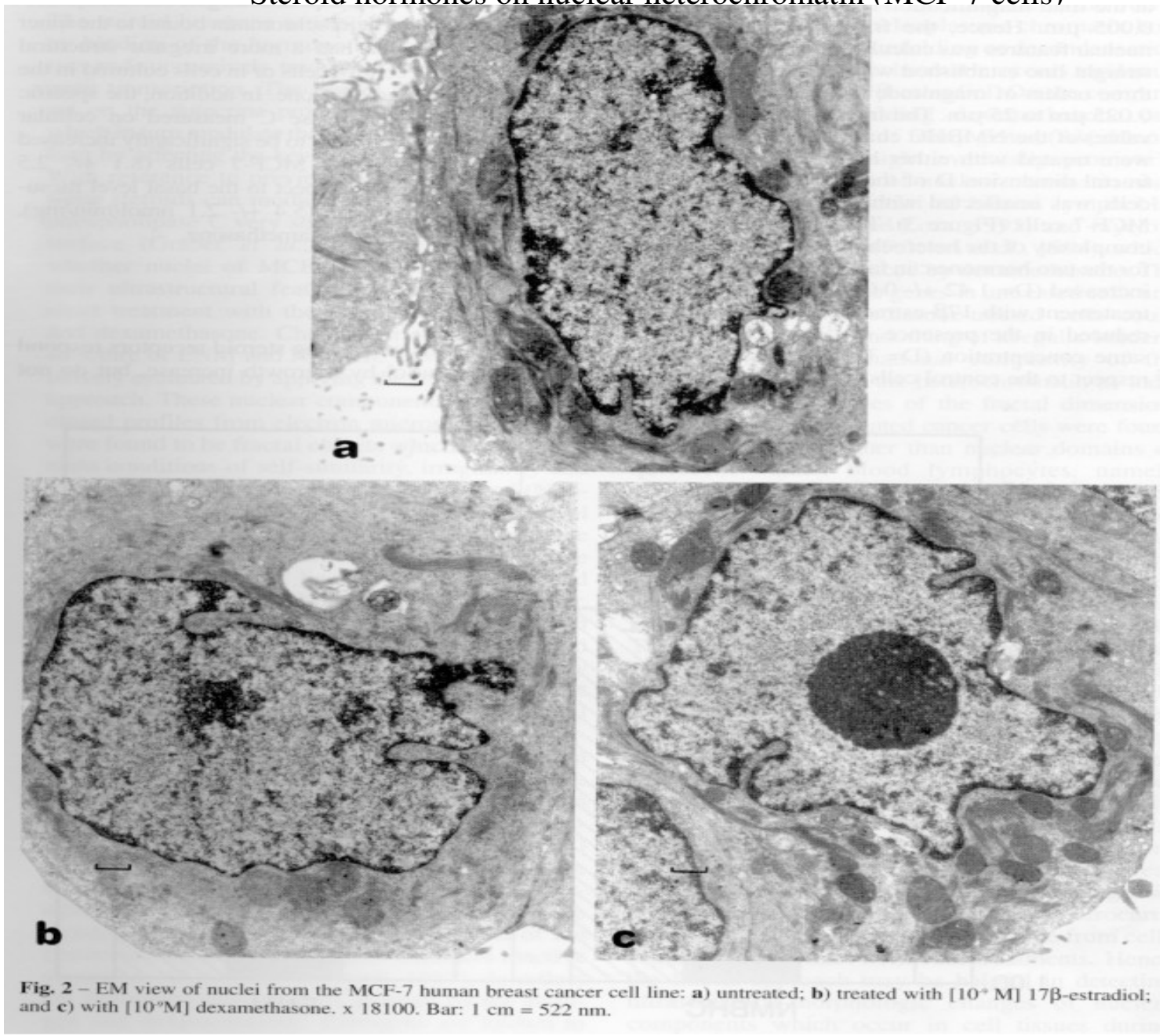

Fig. 2 – EM view of nuclei from the MCF-7 human breast cancer cell line: **a**) untreated; **b**) treated with [10^{-8} M] 17β-estradiol; and **c**) with [10^{-6}M] dexamethasone. x 18100. Bar: 1 cm = 522 nm.

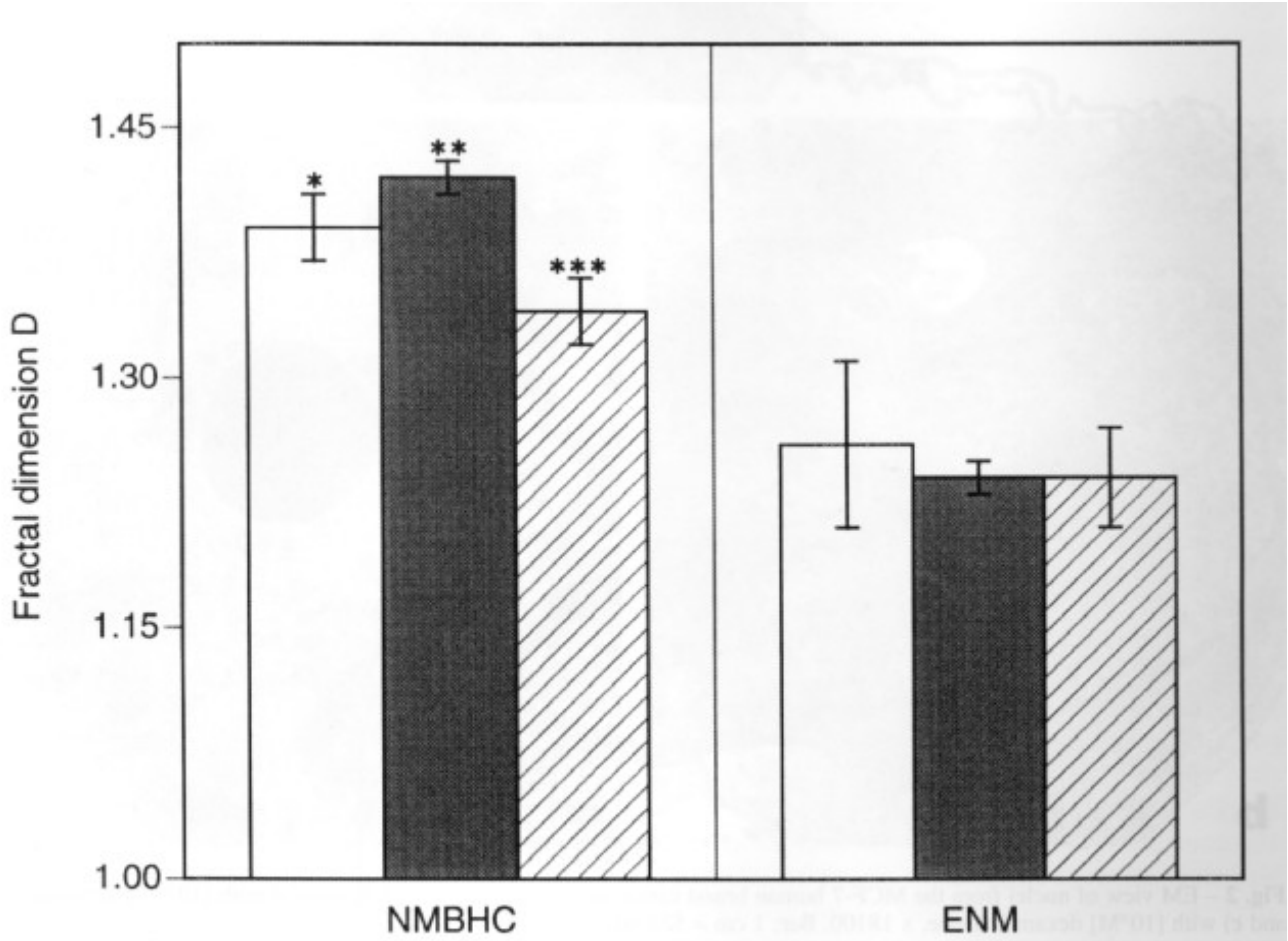

Fig. 3 – Fractal dimension D of nuclear membrane-bound heterochromatin (NMBHC) and external nuclear membrane (ENM) i
untreated (□); [10^{-9} M] 17β-estradiol (■) and [10^{-8}M] dexamethasone (▨)-treated MCF-7 cells. Values given are mean +/
1SD; Significantly different: **/* $p < 0.08$; ***/** $p < 0.01$; ***/* $p < 0.02$.

Apoptosis / Programmed Cell Death

- Physiological form of Cell Death (opposite: necrosis)
- Control of adult tissues and regulation of embryonal development
- Balance between cell proliferation and cell number
- Defense mechanism against damaged, dangerous, and infected cells
- Elimination of cells with altered or endomaged DNA, with mutations or initiatiors of cancers
- Elimination of exhausted cells during tissue and organ developpment (nervous system, immune system, ..)
- Regulation of cell associations within tissues

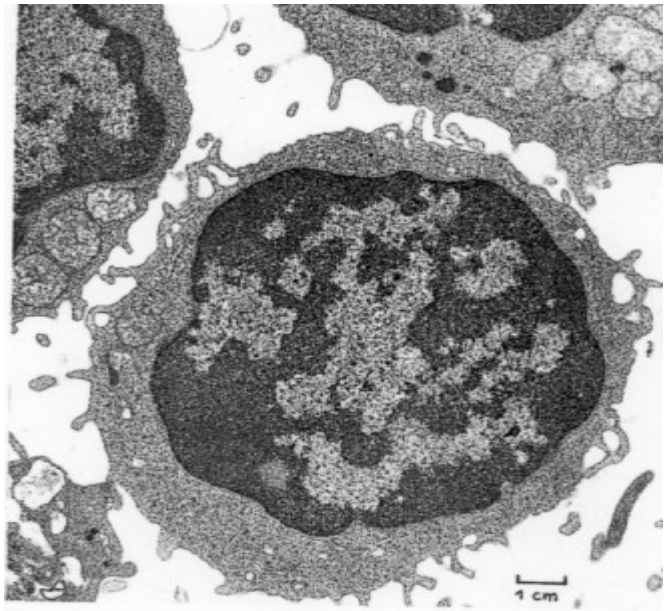

Fig. 1. Linfocito normale. Ingrandimento: 1 cm = 23.000 volt
(435 nm) al microscopio elettronico.

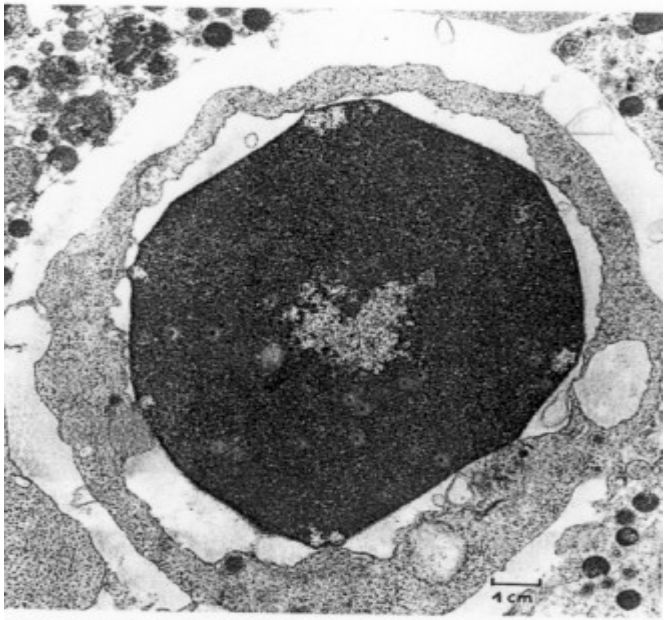

ig. 2. Linfocito in apoptosi al microscopio elettronico. Ingrandi-
ento: 1 cm = 23.000 volte (435 nm).

3.2 Ultrastructural Features of Apoptosis

Quantitative assessment of ultrastructural changes occurring in plasma and perinuclear membranes, although not valuable at a subjective visual inspection, showed that SK-BR-3 cells had entered the initial phases of apoptosis after incubation with 1 μM calcimycin for 24 h (fig 2).

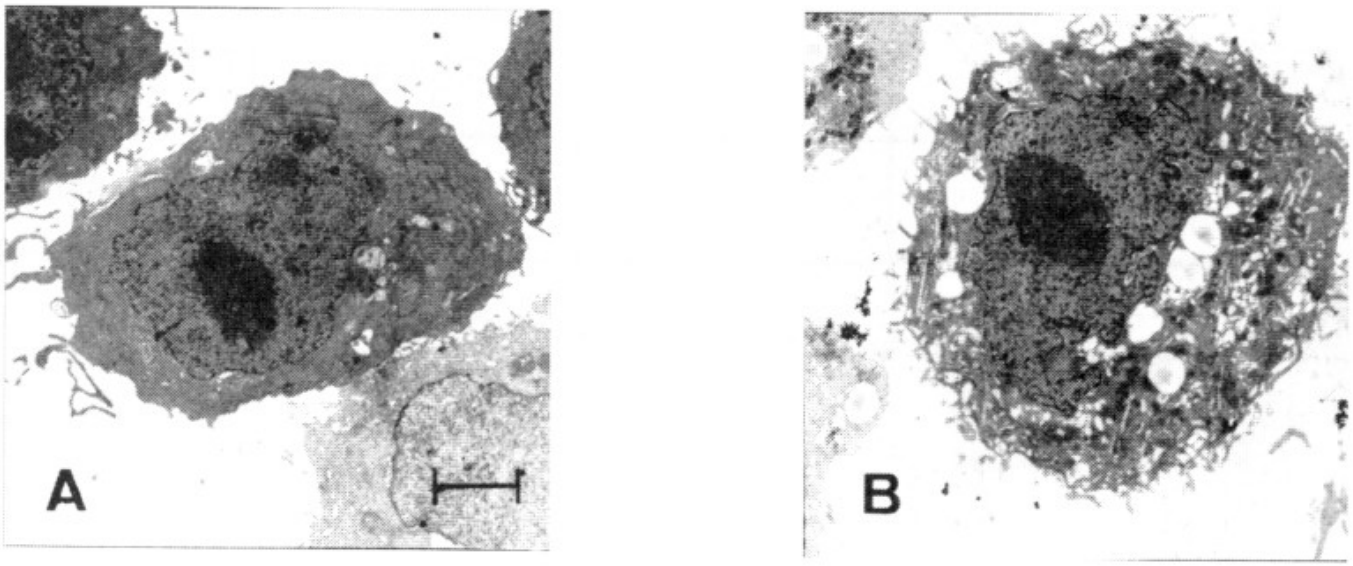

Fig. 2 EM of SK-BR-3 cells, untreated (A) and treated with 1μM A23187 (B) for 24 h. Bar: 1cm = 2.48 μm

Apoptotic markers

Table 1

Time–course expression of membrane and nuclear apoptotic markers in SKBR-3 cells, untreated and treated with 1 μM A23187 Calcimycin

Hours	Plasma membrane markers			
	PI permeability (%)		Annexin-V (%)	
	untreated cells	treated cells	untreated cells	treated cells
0	8.4 ± 2.4	8.4 ± 2.4	4.1 ± 1.8	4.1 ± 1.8
24	13.7 ± 9.2	9.1 ± 0.8	7.3 ± 0.3	8.6 ± 6.6
48	10.3 ± 0.6	27.0 ± 4.3*	5.3 ± 3.2	8.5 ± 6.0
72	6.5 ± 1.0	52.7 ± 13.3**	5.2 ± 4.6	27.9 ± 9.1**
96	10.0 ± 5.2	84.8 ± 3.2**	5.7 ± 0.6	60.1 ± 7.2**

Hours	Nuclear markers			
	TUNEL (%)		Sub G_0/G_1 peak (%)	
	untreated cells	treated cells	untreated cells	treated cells
0	2.6 ± 0.6	2.6 ± 0.6	5.1 ± 1.8	5.1 ± 1.8
24	2.8 ± 0.9	10.4 ± 2.1	3.2 ± 0.4	4.4 ± 1.1
48	2.1 ± 0.5	22.7 ± 3.1**	5.7 ± 0.6	15.4 ± 6.6*
72	2.2 ± 1.3	57.1 ± 6.4**	3.8 ± 0.1	49.7 ± 7.2**
96	3.4 ± 1.0	58.1 ± 8.3**	7.5 ± 3.0	75.3 ± 2.7**

Results (%) are means ± one SD of three separate experiments.

*; ** Significant different at $p < 0.01$ and 0.001, respectively, between untreated and treated cells.

FD of interchromatin space in early apoptotic SK-BR-3 nuclei

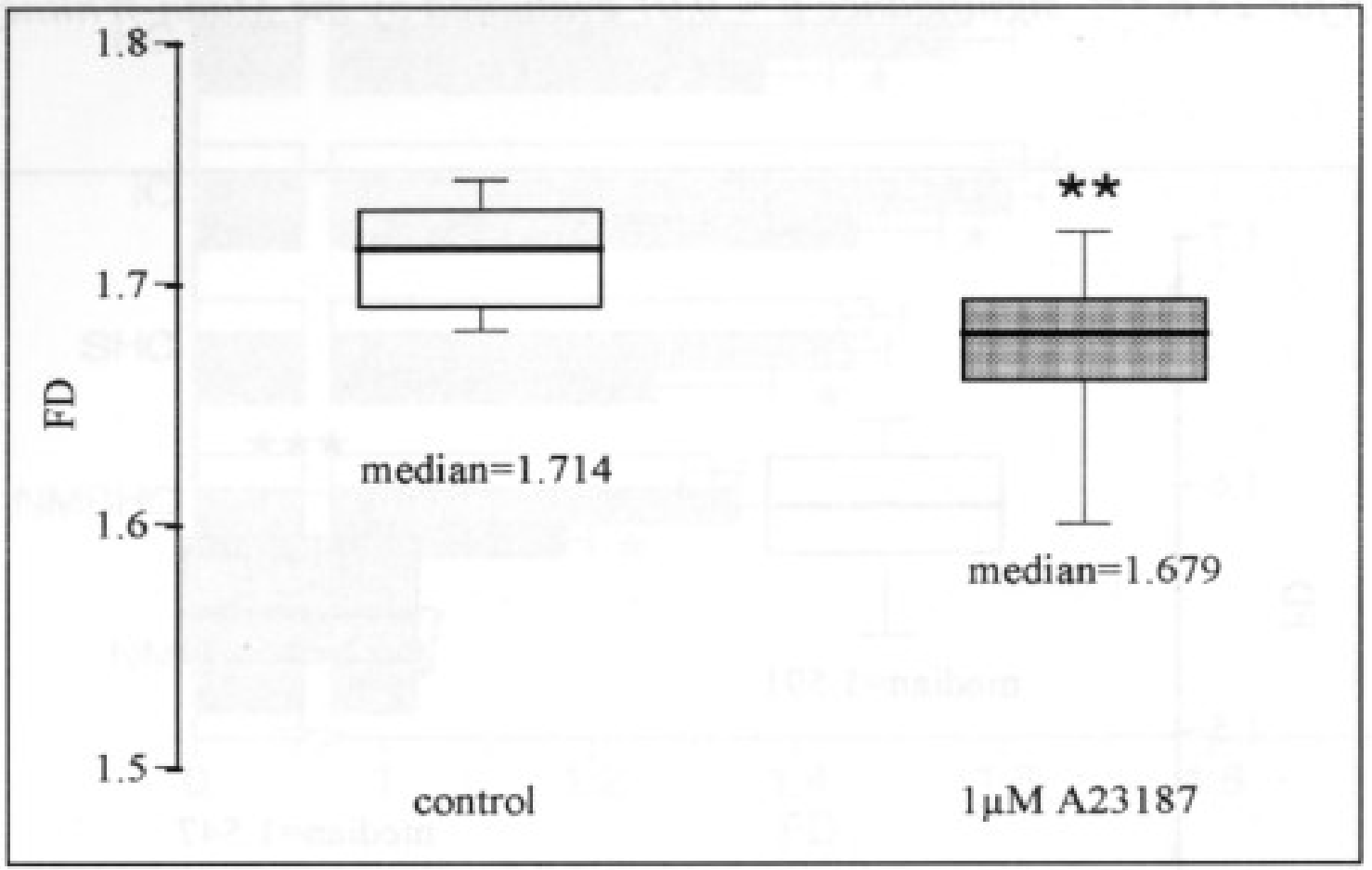

Fractal tree model simulates space-filling branching of airway tree.

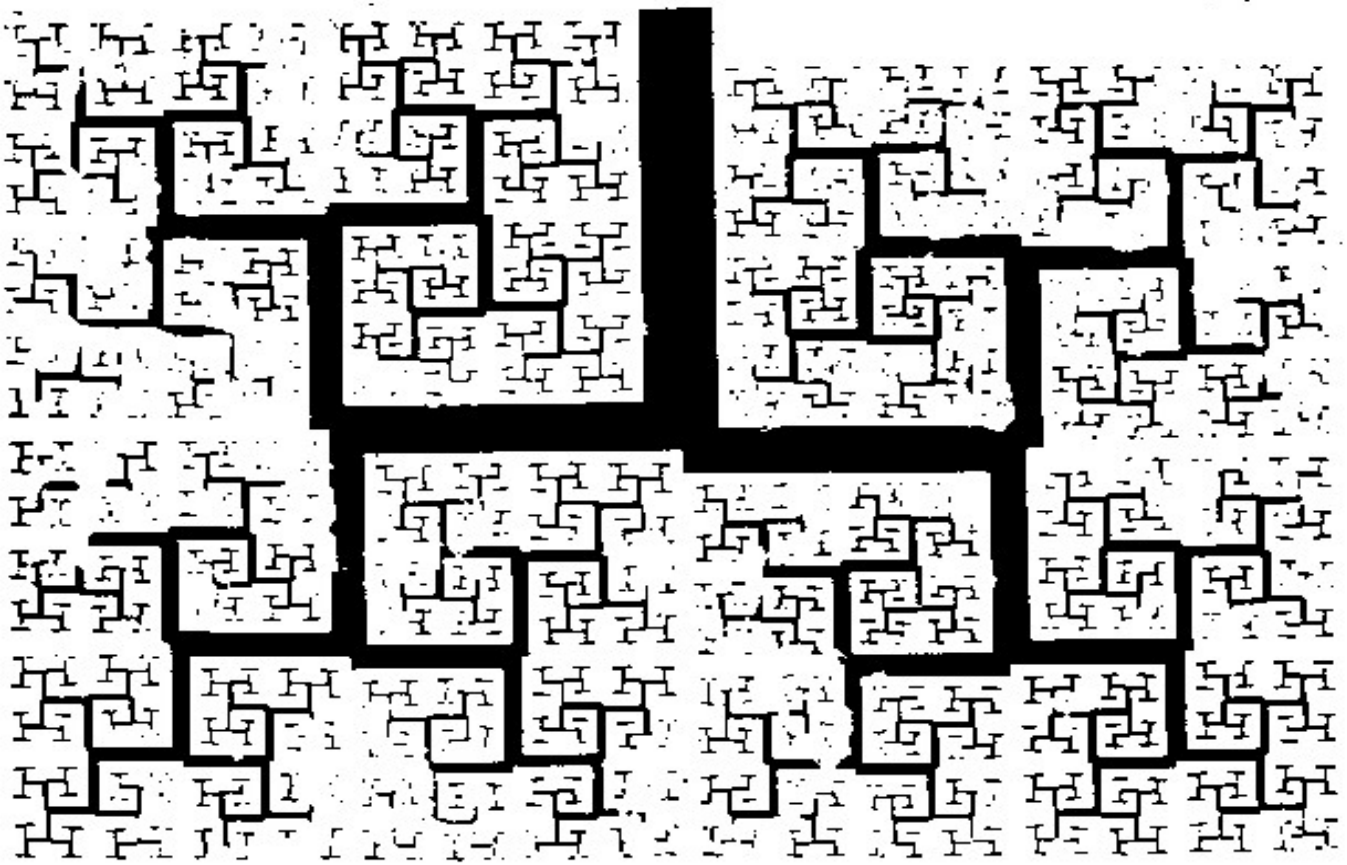

Irregular dichotomous tree with
- paths of different length
- dimensions of the branches: - length and diameter - follow a logarithmic rule in decreasing.

(no legible)

Oocyte with and without Cumulus Oophorus [COC]

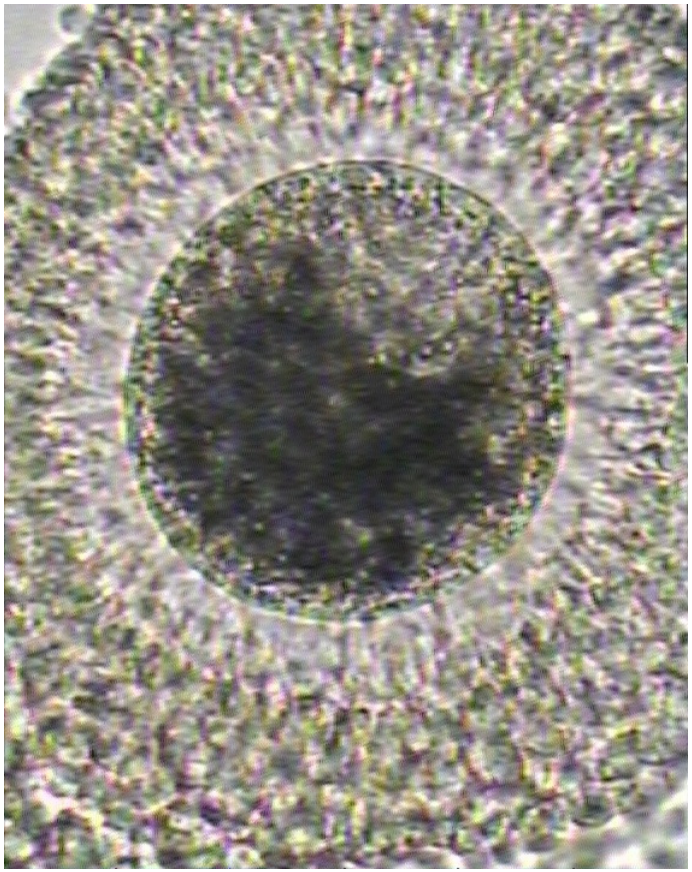

Oocyte grey-dark cytoplasm texture

with COC

without COC

Fractal dimension: methodological comparison

	Oocytes with intact COC			Oocytes without COC		
Image profiles	FANAL	BENOT 1.3	IMAGE-PRO	FANAL	BENOIT 1.3	IMAGE-PRO
Fig.1:D-D1	1,27 ± 0,08	1,19 ± 0,05	1,25 ± 0,09	1,27 ± 0,06	1,19 ± 0,04	1,23 ± 0,05
Fig.1:C-C1	1,54 ± 0,08 **	1,44 ± 0,09	n.m.	1,55 ± 0,11 **	1,43 ± 0,08	n.m.
Fig.1:B-B1	1,91 ± 0,02 *	1,80 ± 0,02	n.m	1,91 ± 0,03 *	1,78 ± 0,01	n.m.

Oocytes with intact COC and successively denuded of COC using finely-drawn glass capillary pipette. A binary image was obtained by grey tresholding the area occupied by the grey-dark of the oocyte cytoplasm (B-B1); two different outlines were extracted from this binary image by applying a Roberts filter: one pertained to the internal texture of the grey-dark cytoplasm area as well as to the scattered grey-dark particles within the cytoplasm (C-C1), while the other referred to the external profile only of the grey-dark cytoplasm (D-D1). Original images of each oocyte were acquired using a 40x objective lens.

Conventional morphometry : tissue percentage distribution
Fractal geometry: irregularity and true surface/ interface

Vv= 100 x Pe/Pt ; Vv = 100 x Pm/ Pt.

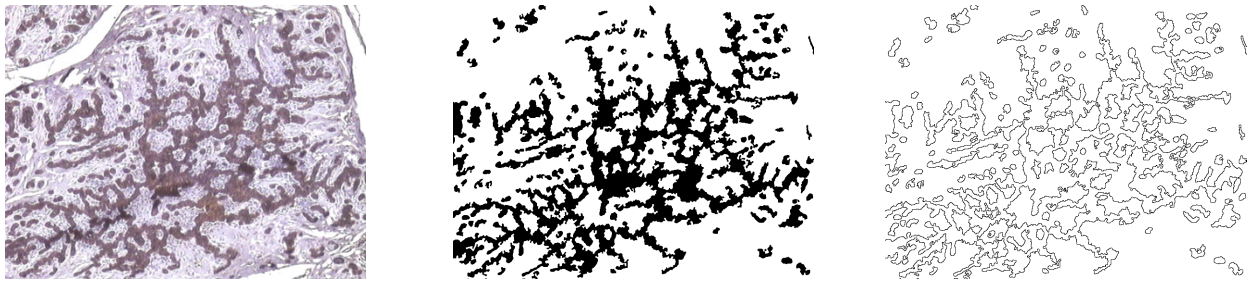

A B C

A) Canine Trichoblastoma: the epithelial component is positive for Cytokeratin, 4X.; B) Binary image obtained by grey thresholding the area occupied by the epithelial component and C) outline of the area occupied by the neoplastic epithelium.

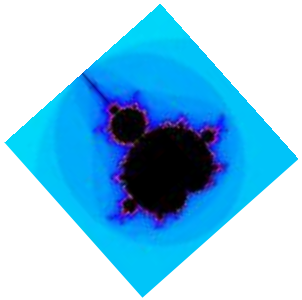

Fractal dimension derived from masks and outlines of canine trichoblastoma

	RT	TT/GC	ST
Mask **Mean** **Sd**	1.75** 0.02	1.85** 0.02	1.78** 0.03
Outlines **Mean** **Sd**	1.70* 0.02	1.77 n.s. 0.02	1.76n.s. 0.02

RT, trichoblastoma of the ribbon type

TT/GCtrichoblastoma of the trabecular and Granular Cellular

ST, trichoblastoma of the spindle

* * significant different at p< 0.001 from each other.

* RT significant different at p< 0.001 from TT/CG and ST .

n.s.: TT/CG ; ST, not significant from each other.

Mouth- ECT interface

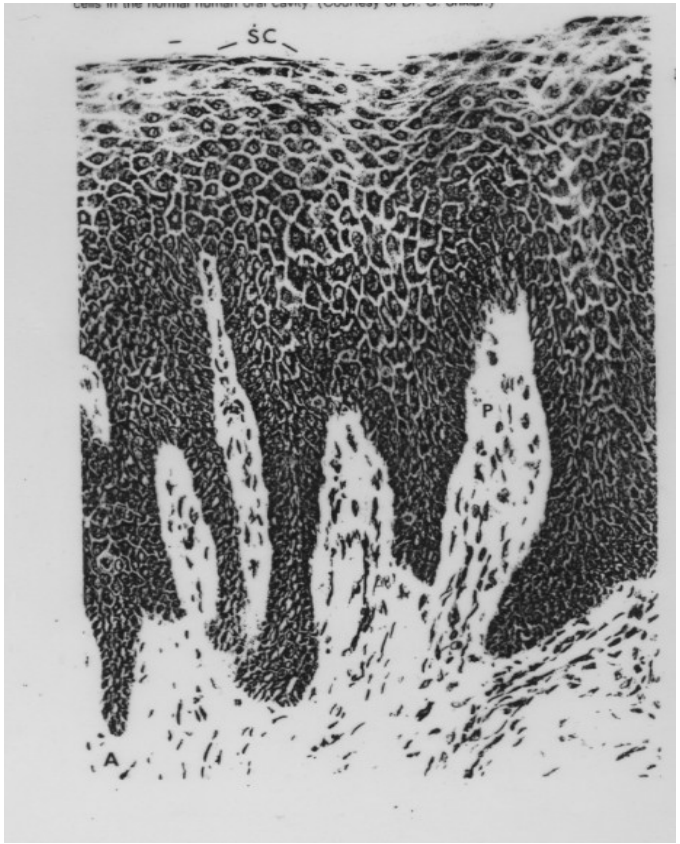

Irregularity (by FD) of Epithelial connective tissue interface [ECTI]

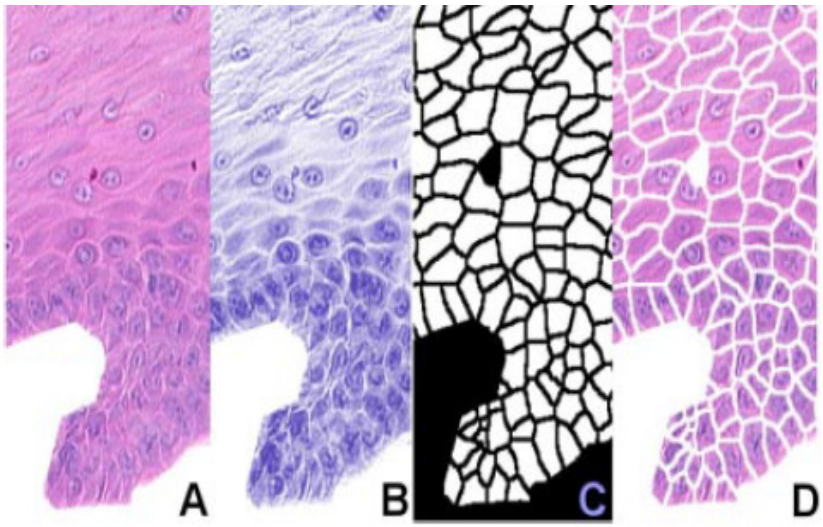

Ageing of the oral mucosa does not seem to affect significantly the irregularity of the epithelial connective tissue interface [ECTI] as documented by close FD values in the table below. A: Image of the epithelium. B: Haematoxylin component of A. C: segmented epithelial compartment. D:segmented epithelial compartment after logical operation between A and C. Magnification 20X.

Mean Box fractal dimension and the number of cases for different age groups.

Age Range	Mean Box Fractal Dimension	Number of cases
0-10	1.1069 ± 0.03267	2
11-20	1.1117 ± 0.08987	2
21-30	1.1414 ± 0.07095	4
31-40	1.1290 ± 0.03822	4
41-50	1.0933 ± 0.05661	5
51-60	1.1373 ± 0.05657	8
61-70	1.0992 ± 0.04456	9
71-80	1.1260 ± 0.04751	5
81-90	1.0903 ± 0.01675	3

Fractal analysis of contours of breast masses in mammograms

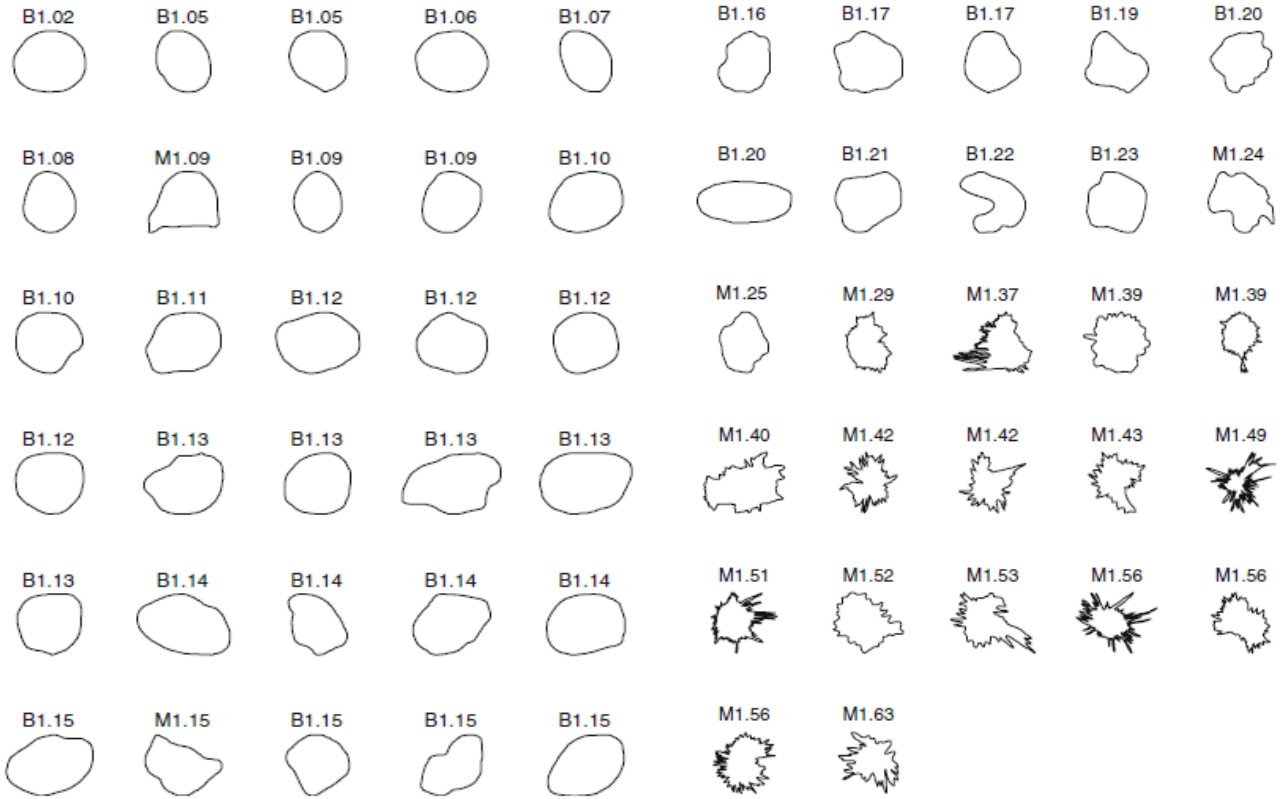

37 benign breast masses and 20 malignant tumors were ranked by their fractal dimension FD estimated by the 1D ruler method.
Rangayyan et al. J Digit. Imag. 2007: 220: 223

Brain and nervous system: a brief chronicle

- **Galeno** (Pergamo) 129-216 d.C.: Conception : superior functions within three cerebral cells (spheres)
  Leonardo 1452-1519: similar conception as Galeno
  Andreas Vesalius 1543: *De humani corporis fabrica* . Cerebral convolutions without identification of morphological pattern
  Marcello Malpighi 1628: (crebral glands; nervous (nerveo) fluid. nerveo) .
  Thomas Willis 1621**:**(arterial circuit by anastomosy of internal carotids and vertebral artery.
  Vicq d'Azyr:1748 :external surface of brain, convolutions , unidentified areas .
  Albrecht von Haller 1708: secretive function of brain, nervous fluid
  Franz Joseph Gall / Johann Spurzheim-1810 : brain shape ----> phrenologic maps with specific function.
  Paul Broca 1861:localization of cerebral functions (langage : "Nous parlons avec 1' hémisphère gauche")
  Carl Wernicke 1874: area of temporal lobe : its damage provokes the sective loss of the capacity of listening words.

- **Camillo Golgi** (1843-1926) ramified nerve fibers could support the **'reticular theory'**, which postulated that the nervous system was a syncytial system, consisting of nervous fibers forming an intricate network, and that the nervous impulse propagated along such diffuse network.

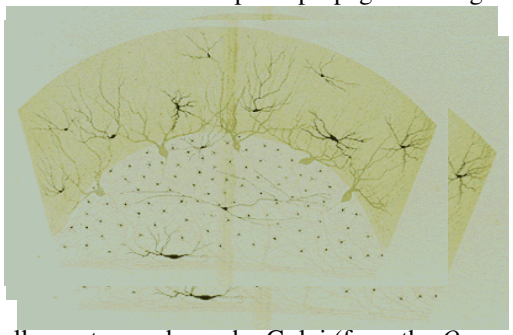

Human cerebellar cortex as drawn by Golgi (from the *Opera Omnia*).

Nervous staining technique: Black reaction: silver nitrate with potassium dichromate-→ black deposit on the soma , axon and dendrites .
Golgi apparatus: Golgi cells of Cerebellum: Golgi 1 (nerve cells with long axons); Golgi II (nerve cells with short or no axons): (GABA: γ-Aminobutyric acid**,** as trasmitter): inhibitor of CNS, regulator of neuronal excitability and muscle tone

- **Santiago Ramón y Cajal**: (1852-1934) "neuron **theory**": the relationship between nerve cells was not one of continuity, but rather of contiguity. Dendritic spine**:** a small membranous protrusion from a neuron's dendrite that typically receives input from a single synapse of an axon (output).
  Cerebellum

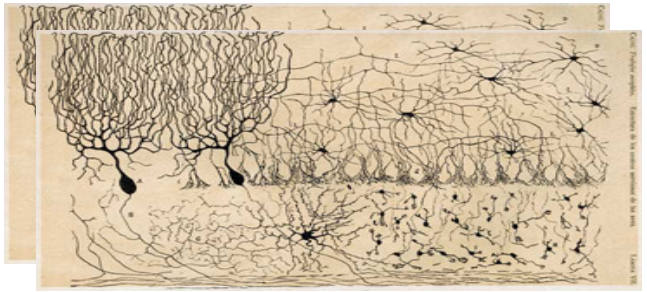

- Techniche di imaging (tomografia ad emissione di positroni; NMR; TAC;

- Analytical description and representation of biological elements
  Mathematics/ statistics / Euclidean geometry/ conventional morphometry
  Fractal Geometry: morphological/ structural complexity: power law scaling , self-similarity

- References:

  M. Piccolino: Breve storia delle Neuroscienze
  Losa GA, T. Nonnenmacher. Self-similarity and fractal irregularity in pathologic tissues. Mod. Pathology 1996:9,174 .
  Losa GA. Fractals in Biology and Medicine. Encyclopedia of Molecular Cell Biology and Molecular Medicine: Systems Biology. 2011, Wiley Press.

Andreas Vesalius (André Vésale)

SECVNDA SEPTIMI LIBRI FIGVRA.

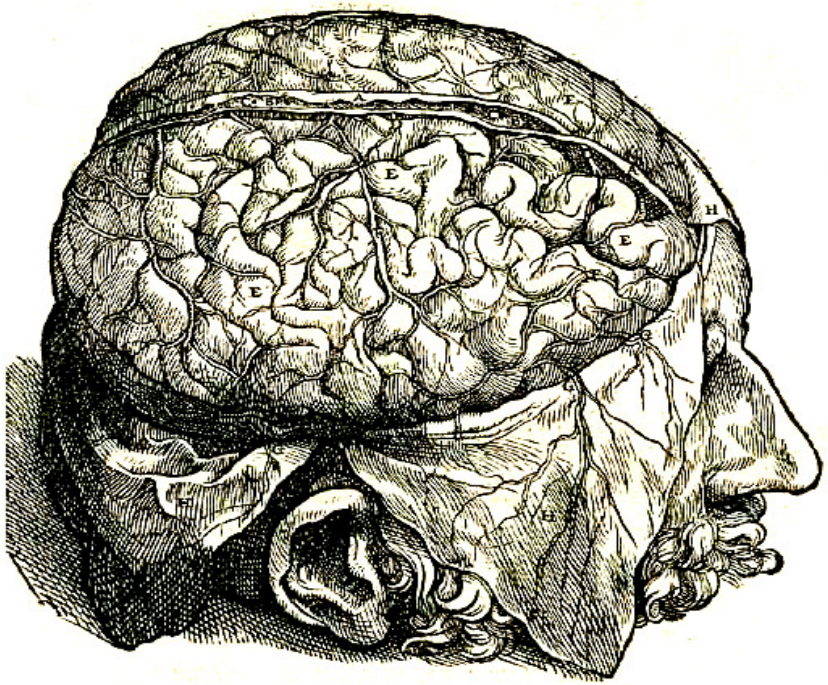

SECVNDAE FIGVRAE, EIVSDEMQVE CHARA-
cterum Index.

PRAESENS figura ſectionis ſerie primam ſubſequens, tertium duræ membranæ ſinum (quem prima figura C aliquot inſignitum gerit) longa ſectione ſecundùm capitis longitudinem ducta adapertum commonſtrat. Inſuper ad huius tertij ſinus latera, per capitis quoq; longitudinem duas deduxi ſectiones, utrinque nimirũ ad ſinum ſingulas, quæ duram membranam duntaxat penetrarunt, & duræ membranæ latera ab ea membranæ ſeparariũt parte, quæ dextram cerebri partem à ſiniſtra dirimit, atque in ſubſequẽti figura tribus D inſignietur. Præter tres iam cõmemoratas ſectiones utrinque aliã quoque molitus ſum, quæ ab aure ad uerticẽ pertingẽs, ſolam

The major portions of the Brain : Cerebrum, Cerebellum, Brain Stem

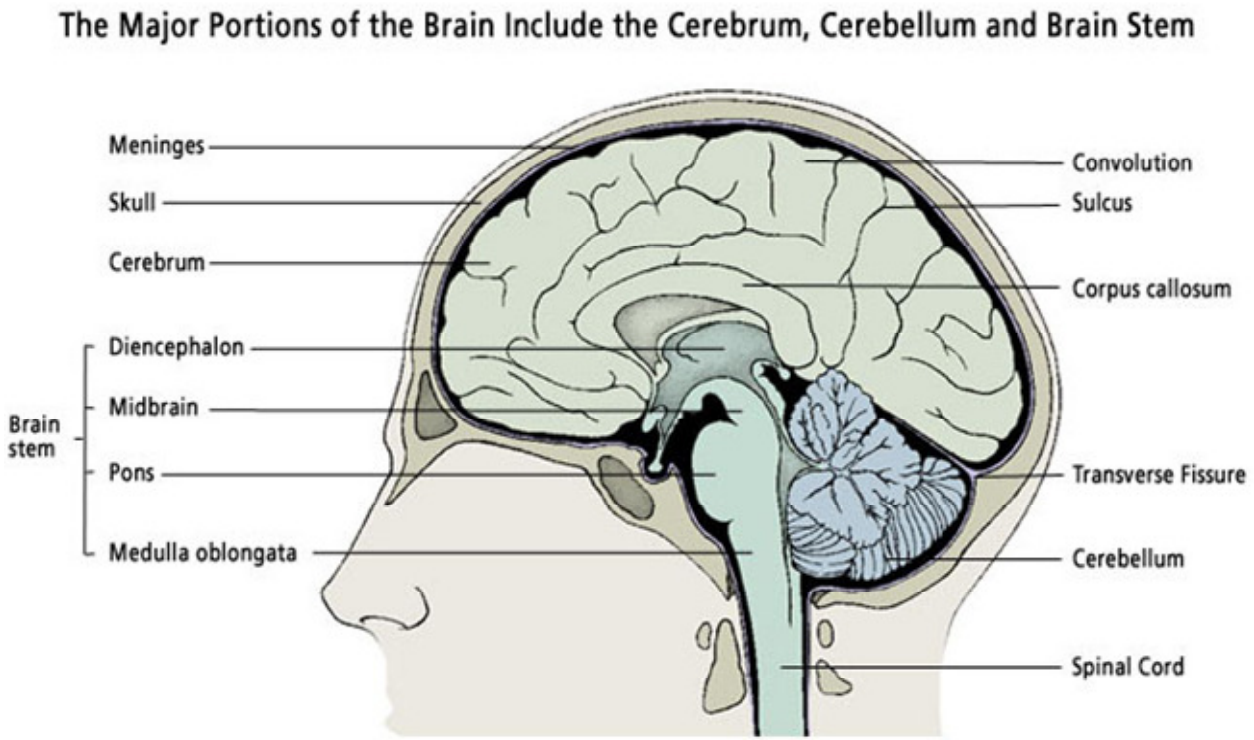

Brain complexity

1-month and 6-year-old-child

Increase in brain size and the maturation of cortical circuits

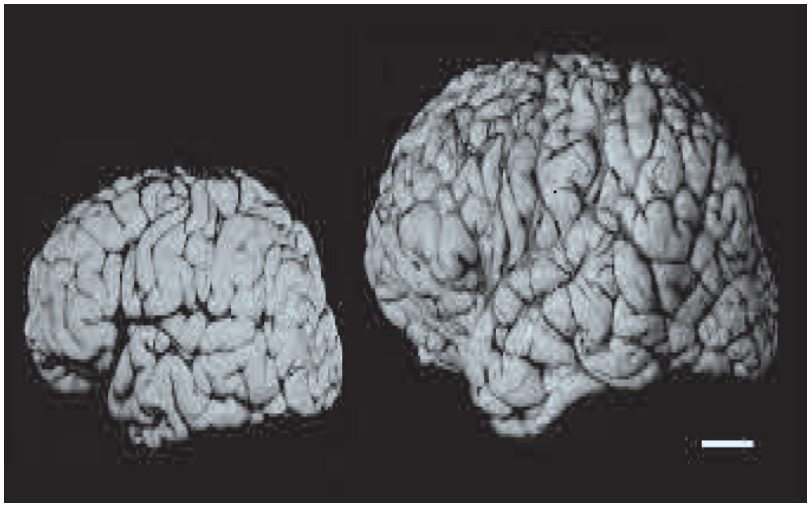

Golgi stained cortical neurons of orbital gyrus

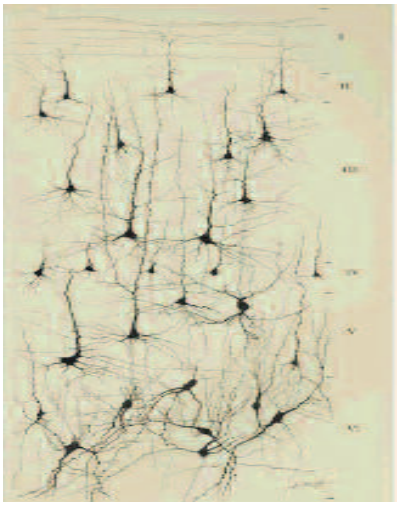

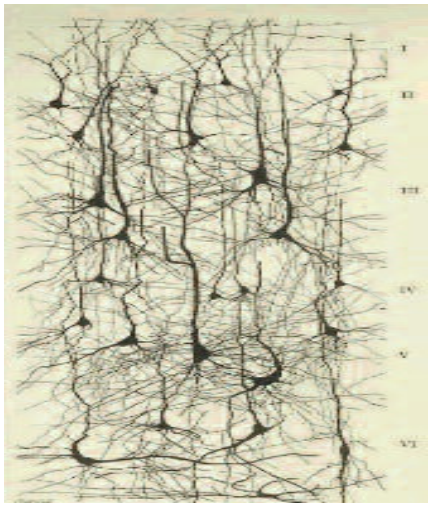

J. De Felipe: The evolutionary concourse of two major events, “the tremendous expansion and the differentiation of the neocortex,”, has contributed to the development of the human brain. J. Front. Neuroanatomy 2011, 5, 1-16

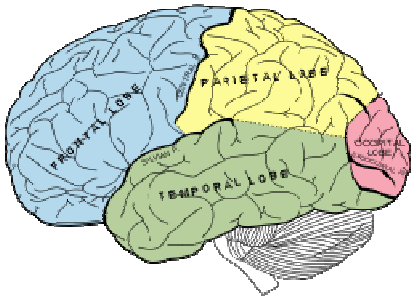

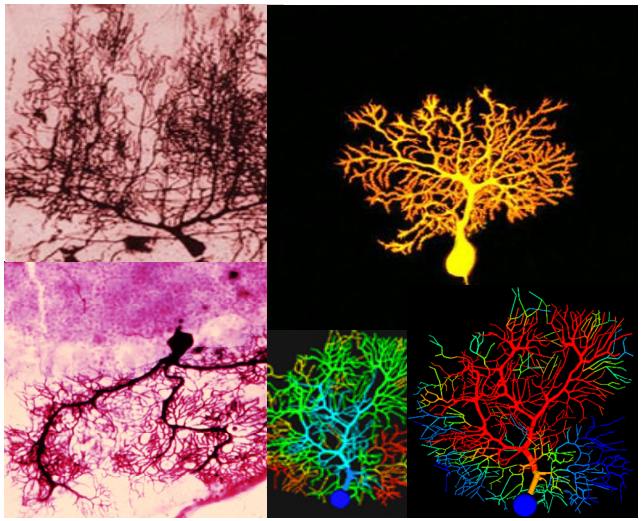

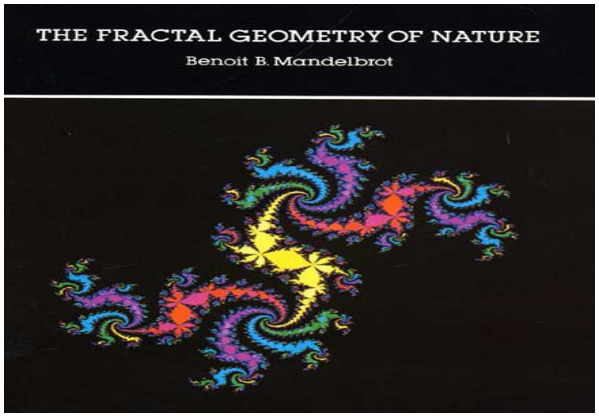

1982. In his masterpiece - ***The Fractal Geometry of Nature*** -

Mandelbrot, facing with the intricacy of mammalian brain folds, argued:

< A quantitative study of such folding is beyond standard geometry but fits beautifully in fractal geometry >

At that time however, there was no certainty neither about the brain's geometry nor the neuron branching. The anatomy-histological evidence that the complexity of plane-filling maze formed from dendrites of neural Purkinje cells of cerebellum was more reduced in non mammalian species than in mammals led up Mandelbrot to comment:

< It would be very nice if this corresponded to a decrease in D (fractal dimension), but the notion that neurons are fractals remains conjectural >

Since then, a wealth of investigations have documented the fractal organization of brain and nervous tissue system while the implication of fractals for neurosciences was unambiguously assessed.

Pyramidal neuron

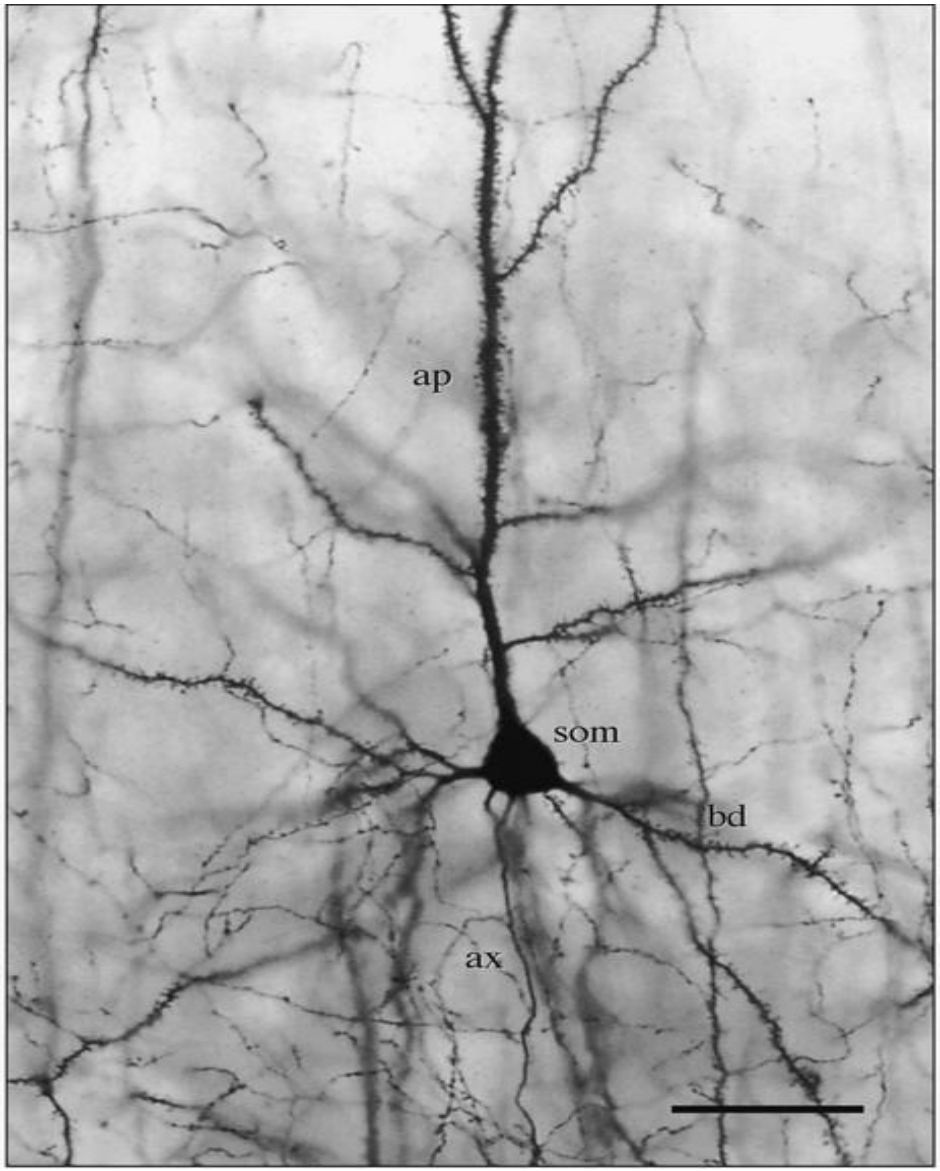

Fractal Self-Organization:Purkinje Cells in Cerebellum

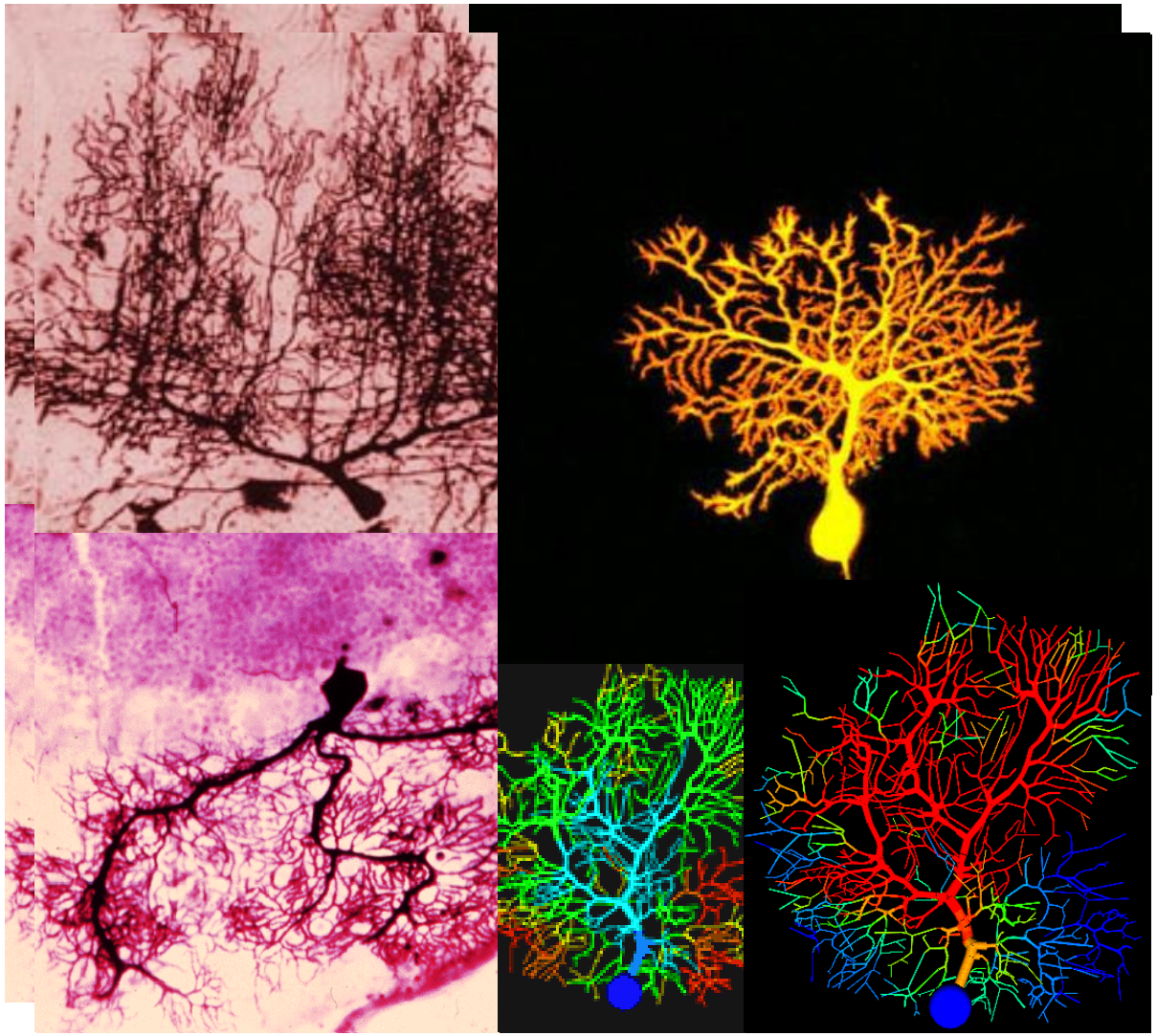

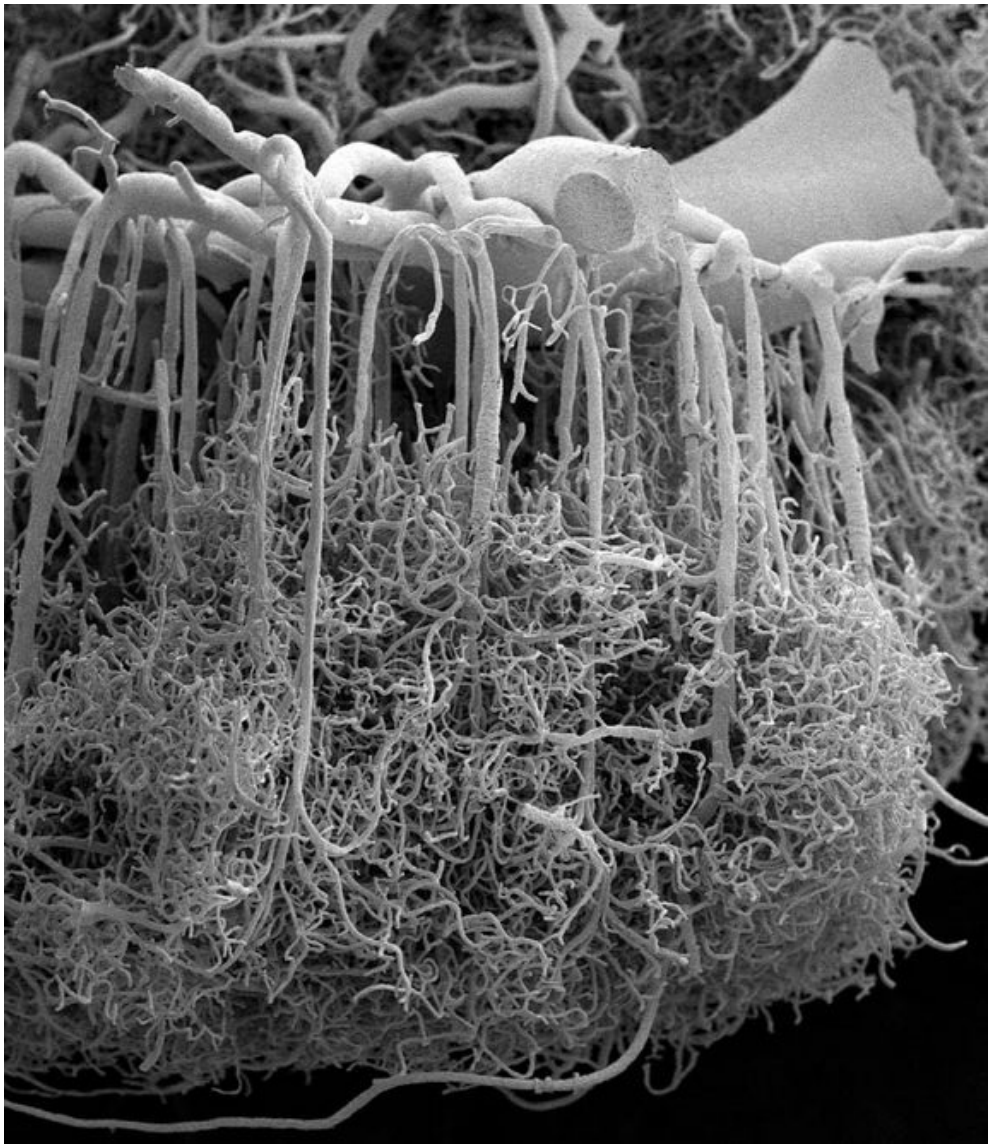

Nervous fibers of white matter rebuild by IRMf (functional Resonance Magnetic Imaging)

The Geometric Structure of the Brain Fiber Pathways

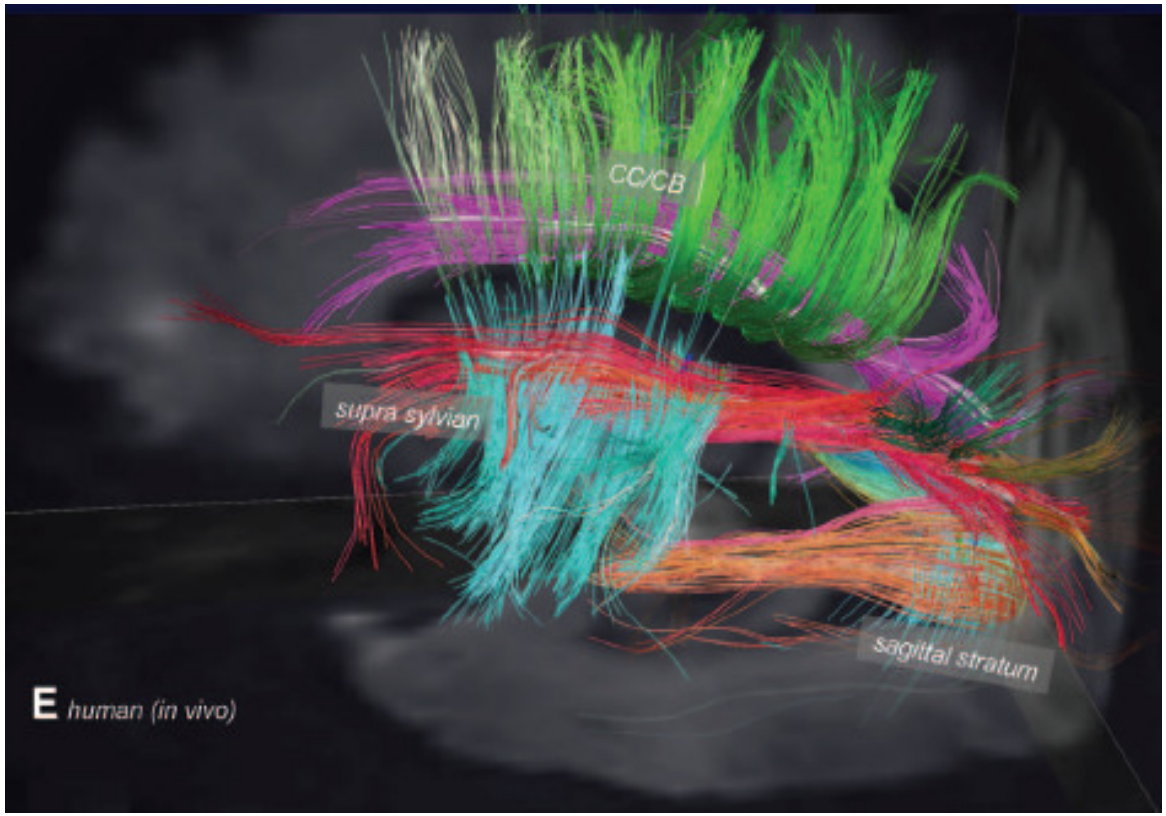

The organizing principles of cerebral connectivity remain unclear and difficult to correlate with the structure of brain. In the brainstem and spinal cord, fiber pathways are organized as parallel families derived from the three principal axes of embryonic development: the rostro-caudal, the medio-lateral (or proximo-distal), and the dorso-ventral. Several leading theories of cerebral function propose geometric organization at multiple scales. However, high-resolution studies of cerebral connectivity with tract tracers have given only limited evidence of geometric organization.(Van Weeden et al.2012.

NMR

- 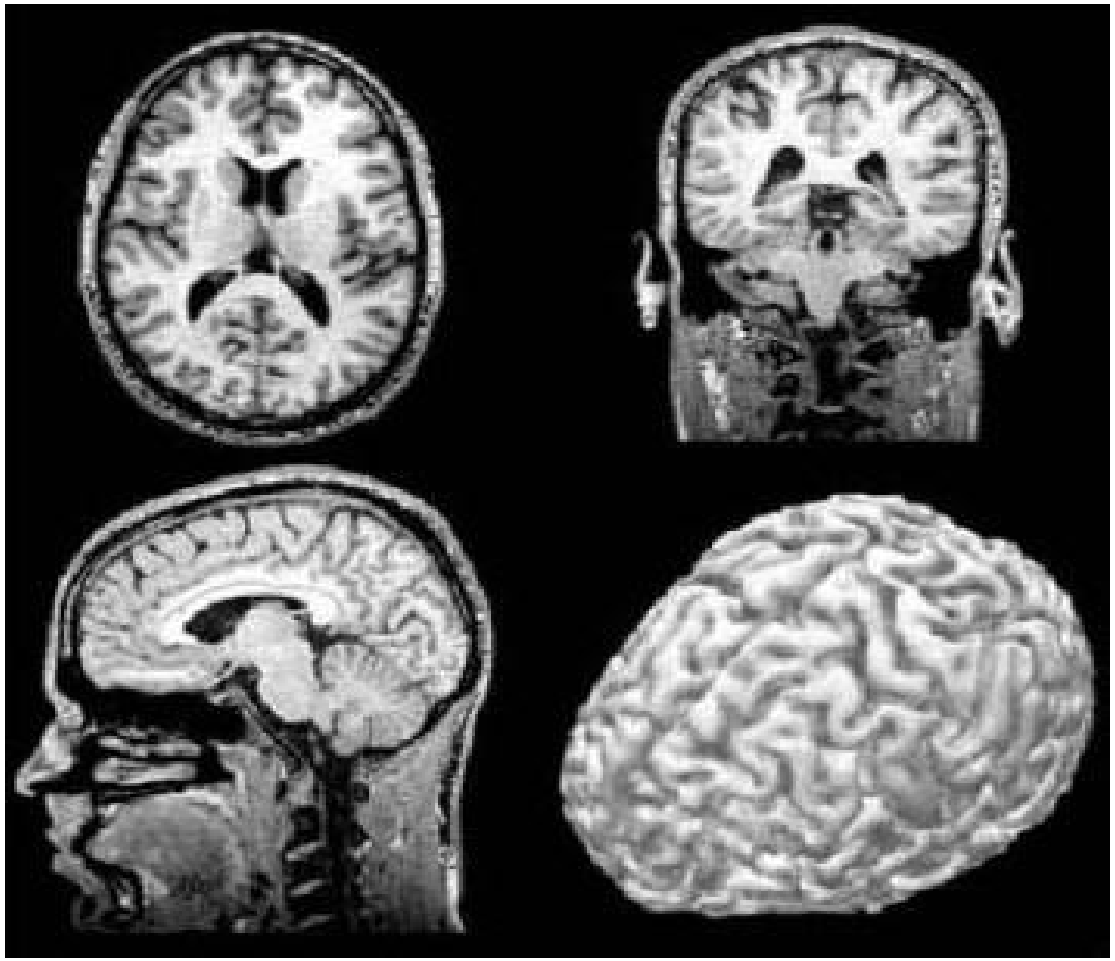

The neocortical column microcircuit

Markram H. The Blue Brain Project. Perspectives. Nature reviews 7, 2006

a b c d

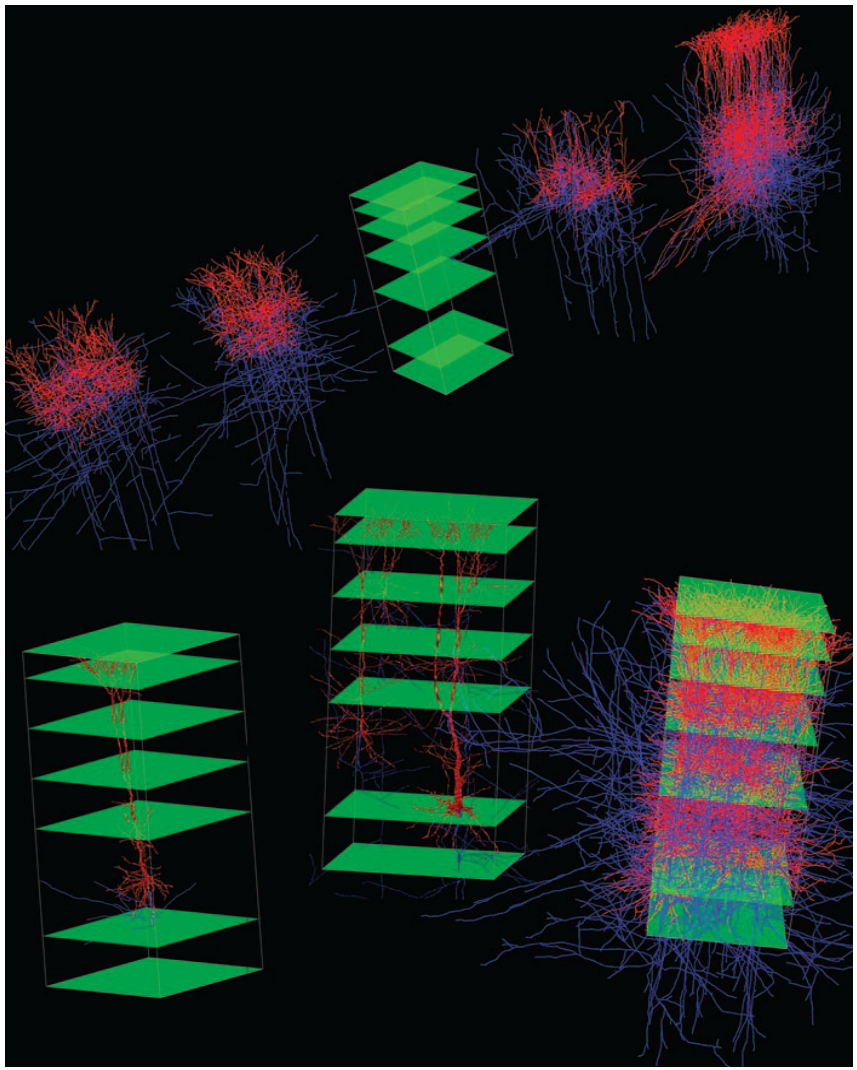

Morphological development of thick-tufted layer V pyramidal cells in the rat somatosensory cortex (conventional morphometry)

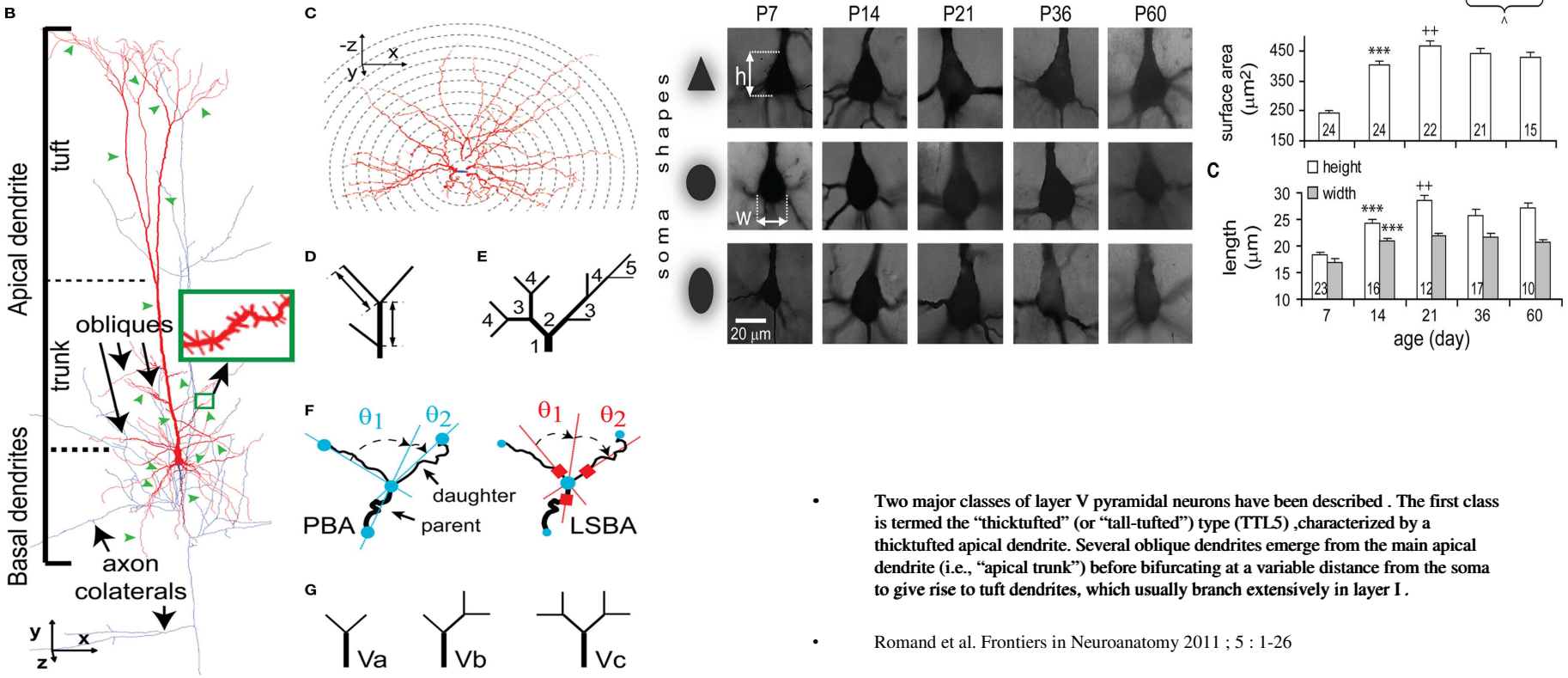

- **Two major classes of layer V pyramidal neurons have been described . The first class is termed the "thicktufted" (or "tall-tufted") type (TTL5) ,characterized by a thicktufted apical dendrite. Several oblique dendrites emerge from the main apical dendrite (i.e., "apical trunk") before bifurcating at a variable distance from the soma to give rise to tuft dendrites, which usually branch extensively in layer I .**

- Romand et al. Frontiers in Neuroanatomy 2011 ; 5 : 1-26

Neuronal images FD

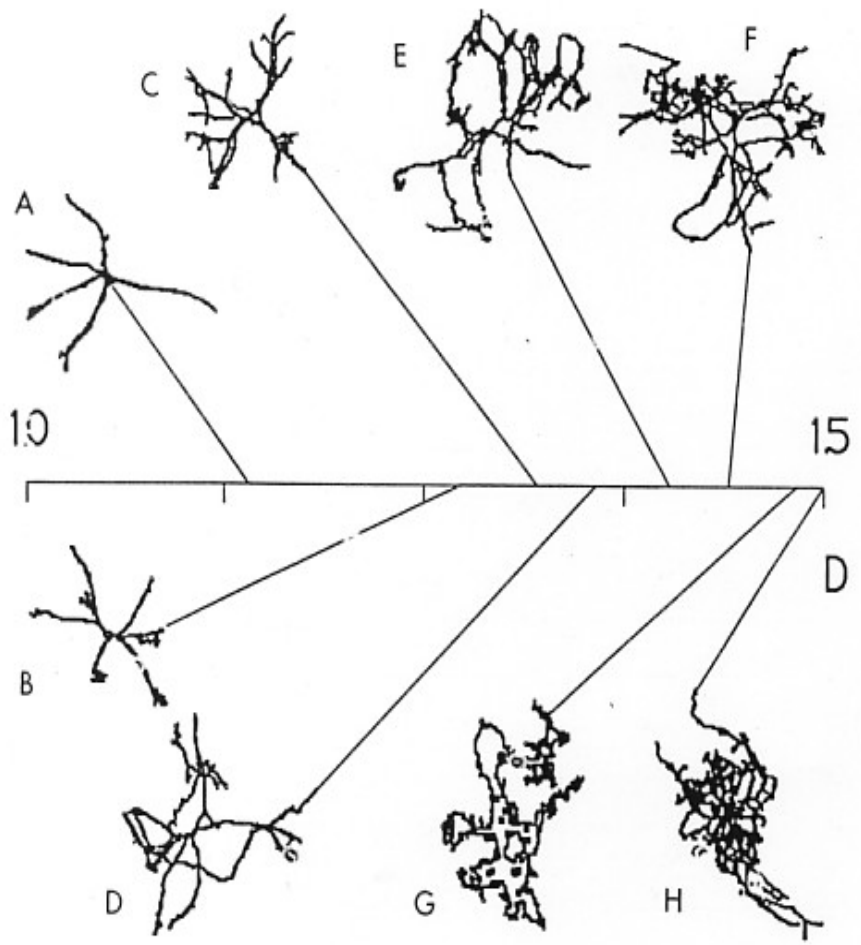

Fig. 2 A set of neuronal images ordered by increasing fractal dimension. The value of D for each image is indicated by its position on the D axis. Visually perceived morphologic complexity correlates well with estimated fractal dimension. Reprinted with permission from Smith et al., 1989.

FD (box-counting method) of Dendritic Branching Pattern

Milosevic et al.. J.Theor. Biology 2009, 259, 142

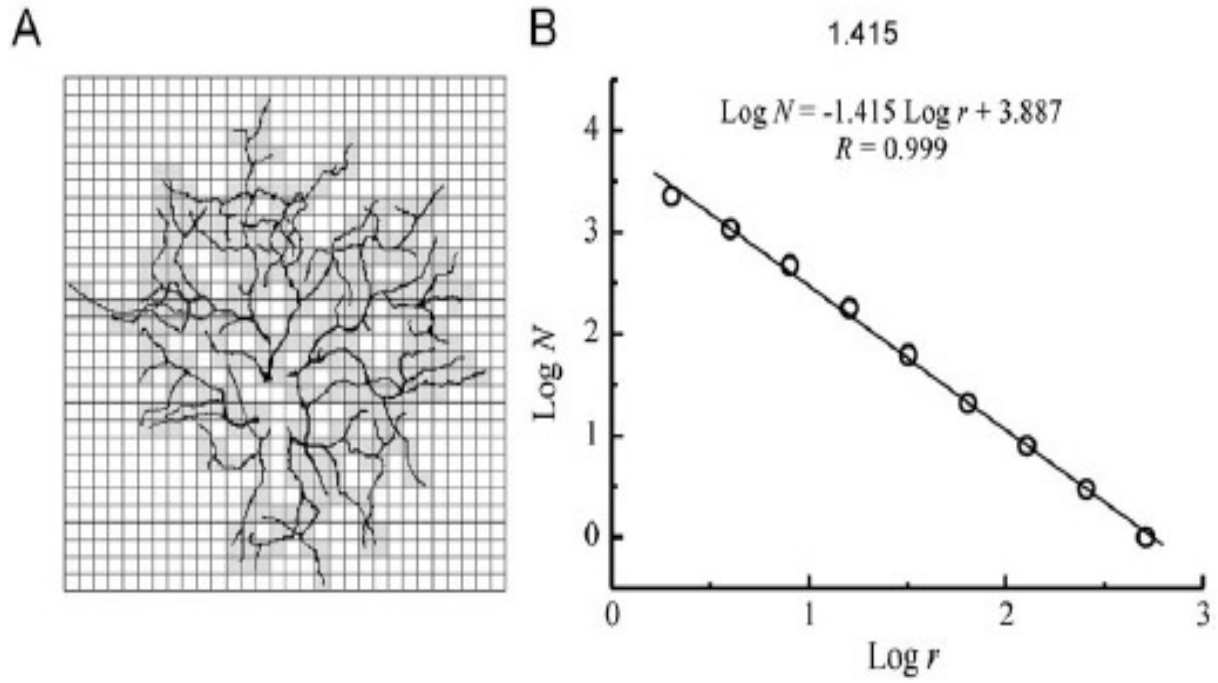

Fig. 2. Camera-lucida drawings of young multipolar astrocytes from neonatal brain. The fractal dimensions D of the cells are, (A) = 1.46; (B) = 1.35; (C) = 1.42; (D) = 1.37; (E) = 1.32; (F) = 1.42. For easier comparison, Figures 2 to 5 are given at the same calibration.

D= 1.32 — 1.46

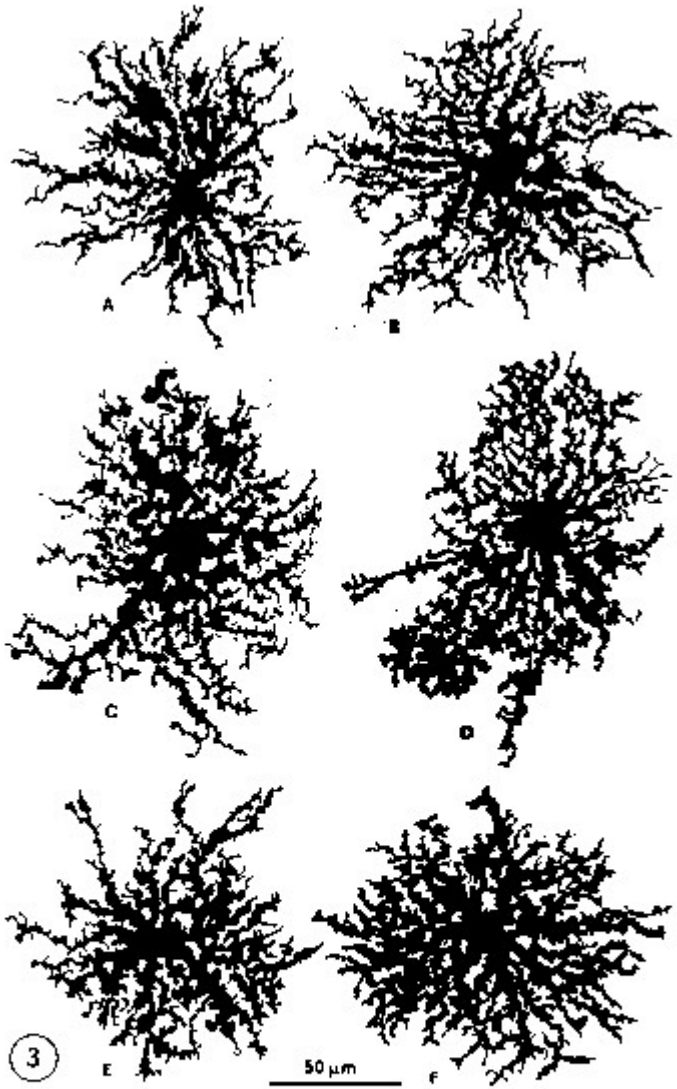

3

Fig. 3. Camera-lucida drawings of astrocytes from normal adult brain. The fractal dimensions D of the cells are: (A) = 1.57; (B) = 1.61; (C) = 1.59; (D) = 1.56; (E) = 1.56; (F) = 1.60.

D= 1.56 - 1.61

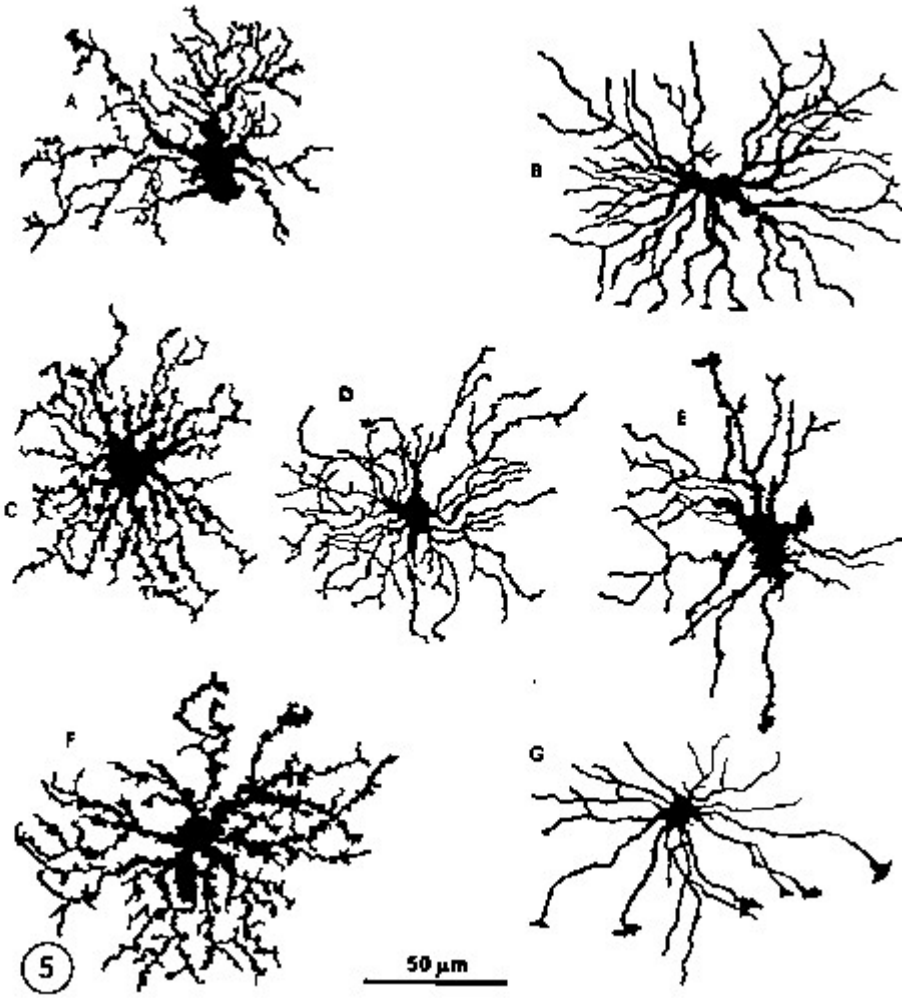

Fig. 5. Camera-lucida drawings of astrocytes from brain of a patient suffering from dementia. The fractal dimensions D of the cells are, (A) = 1.49; (B) = 1.49; (C) = 1.52; (D) = 1.50; (E) = 1.41; (F) = 1.52; (G) = 1.39.

D = 1.39-1.52

Fractal analysis of astrocytes in stroke and dementia

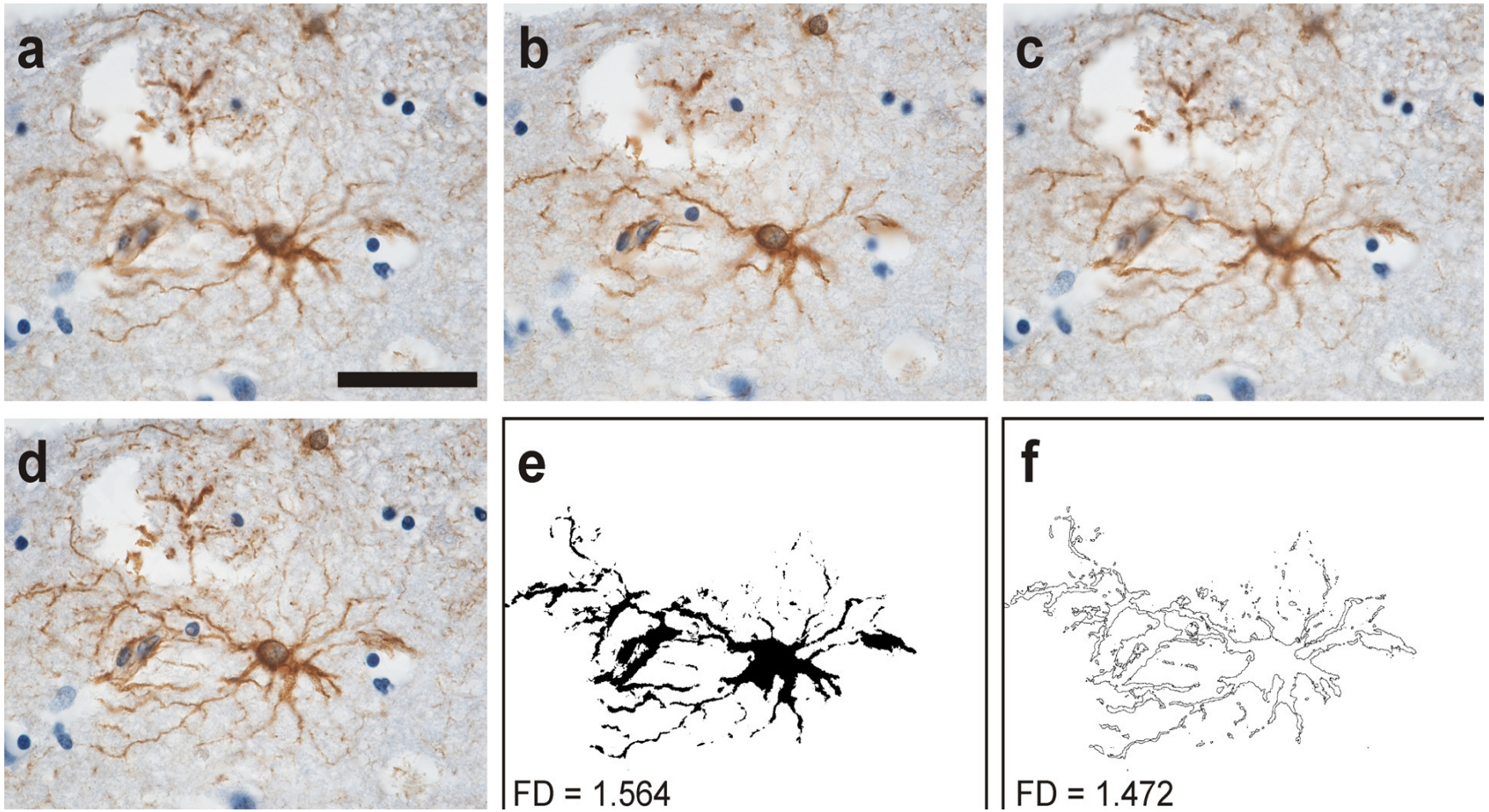

Figure 2. Typical illustration of 2D WM skeleton superimposed on an anatomical T1-weighted images.

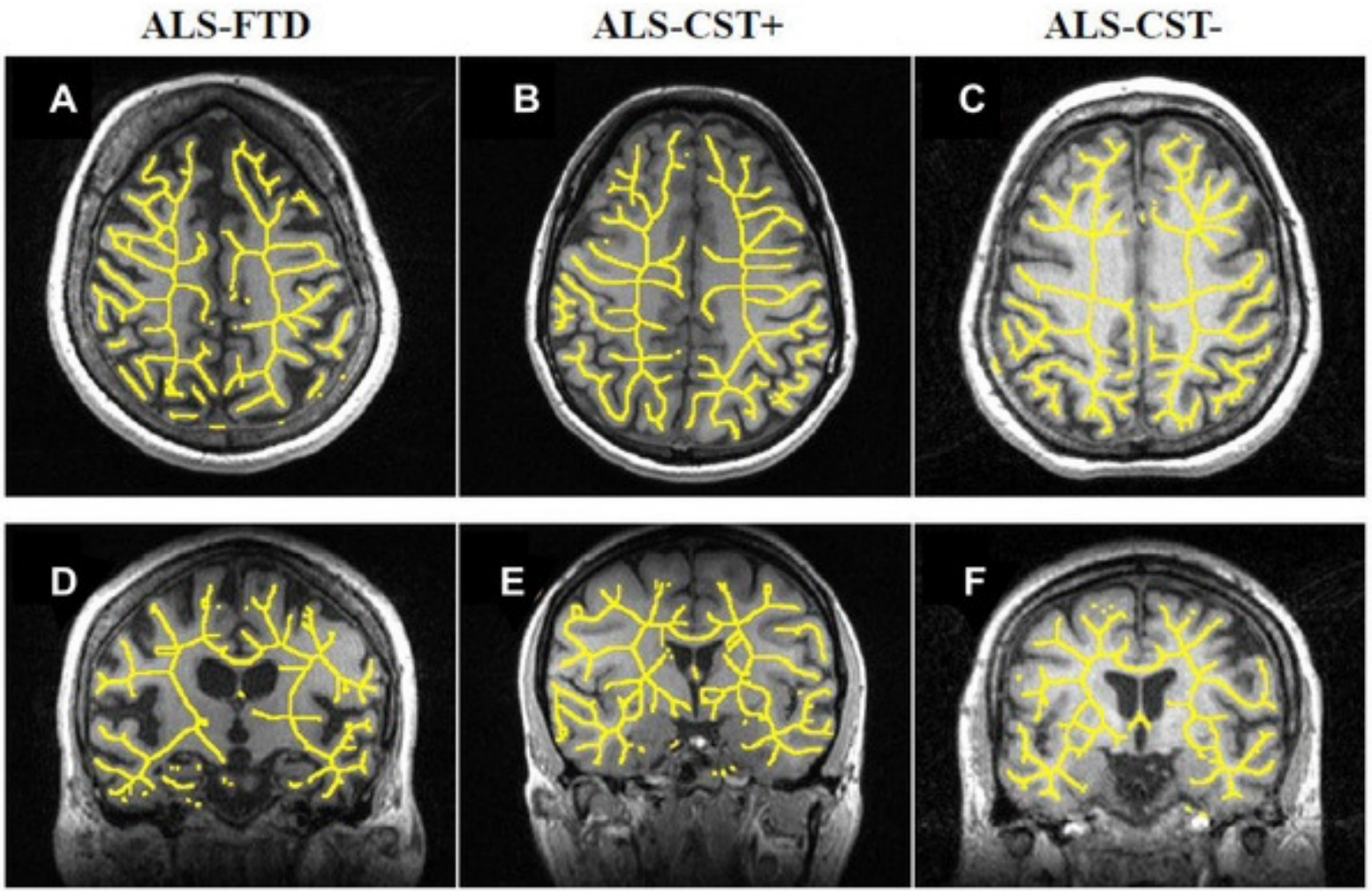

Rajagopalan V, Liu Z, Allexandre D, Zhang L, et al. (2013) Brain White Matter Shape Changes in Amyotrophic Lateral Sclerosis (ALS): A Fractal Dimension Study. PLoS ONE 8(9): e73614. doi:10.1371/journal.pone.0073614
http://www.plosone.org/article/info:doi/10.1371/journal.pone.0073614

Fractal dimension analysis of grey matter in multiple sclerosis (3D)

Grid classification for a 3D image composed of 156 2D slices of segmented grey matter with a threshold of 1 and for two different box sizes: 2 (A) and 5 (B); due to the 3D representation, all boxes shown are classified as GREY. Boxes of sizes 2 (C) and 5 (D) for only one row of the total classification, where the box classification in BLACK (blue colour), WHITE (empty colour) and GREY (green colour) is clearly shown. (E) Example of 3D fractal dimension computation through linear regression over the box counting; the range selected for the linear regression is the set of green points (box sizes from 6 to 16);red points are the box counting of box sizes not selected for the final computation

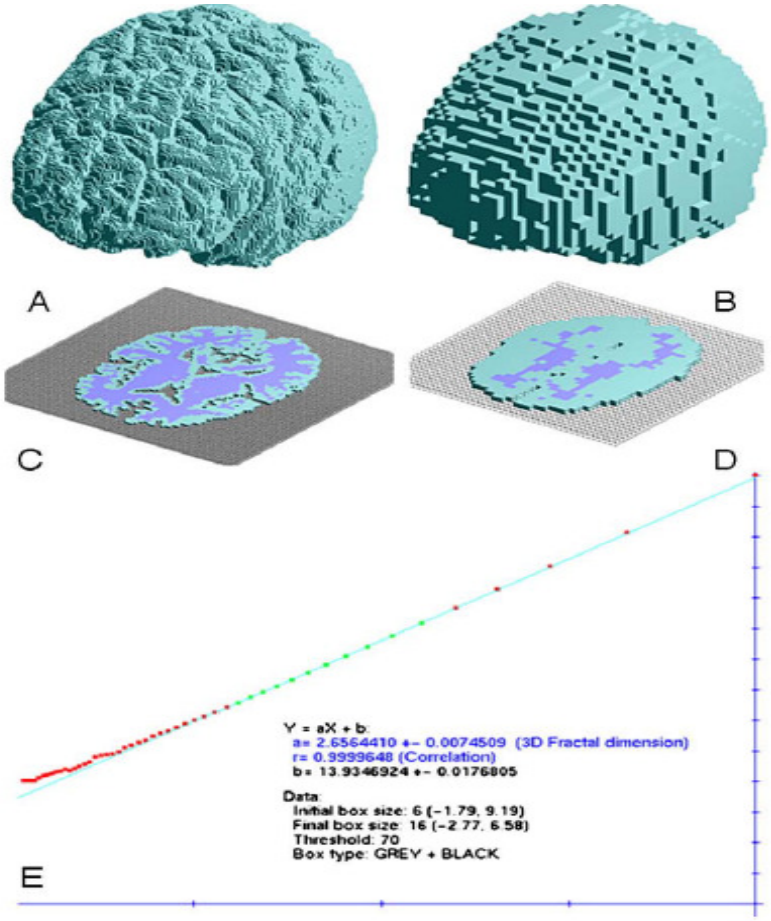

Fractal dimension (FD) of the grey matter (GM) form controls and MS patients

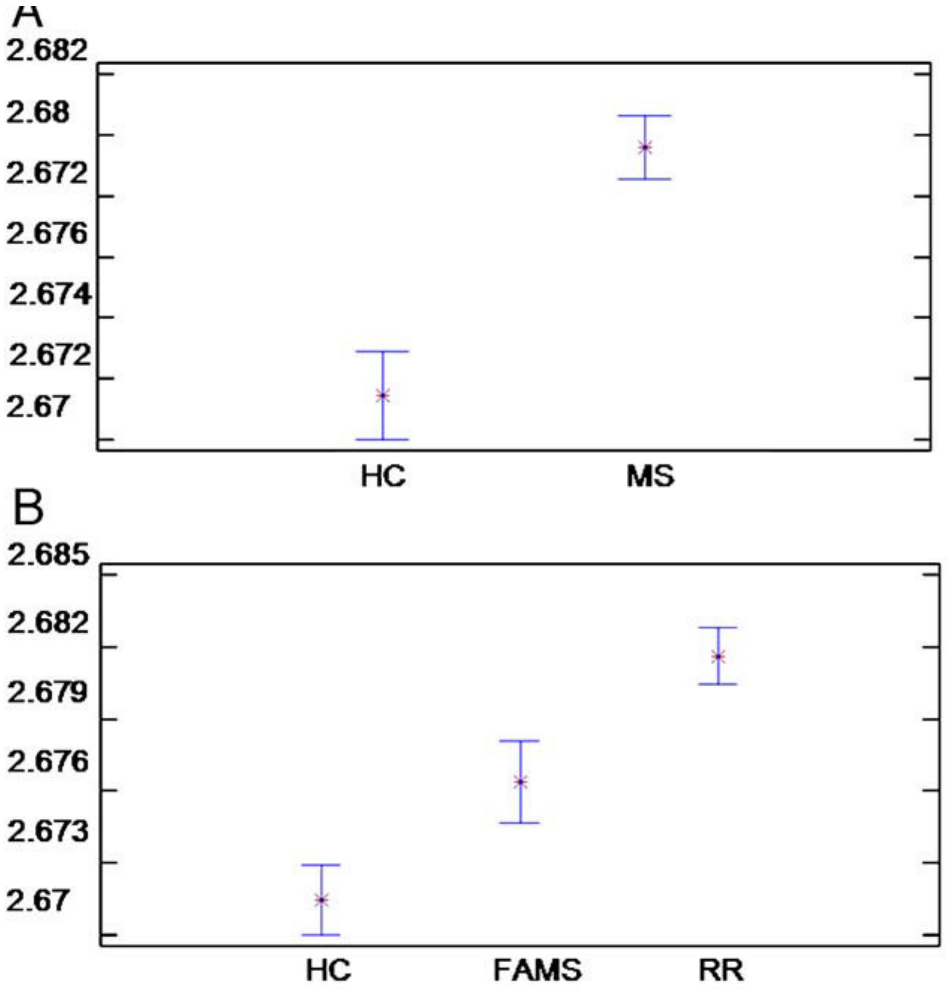

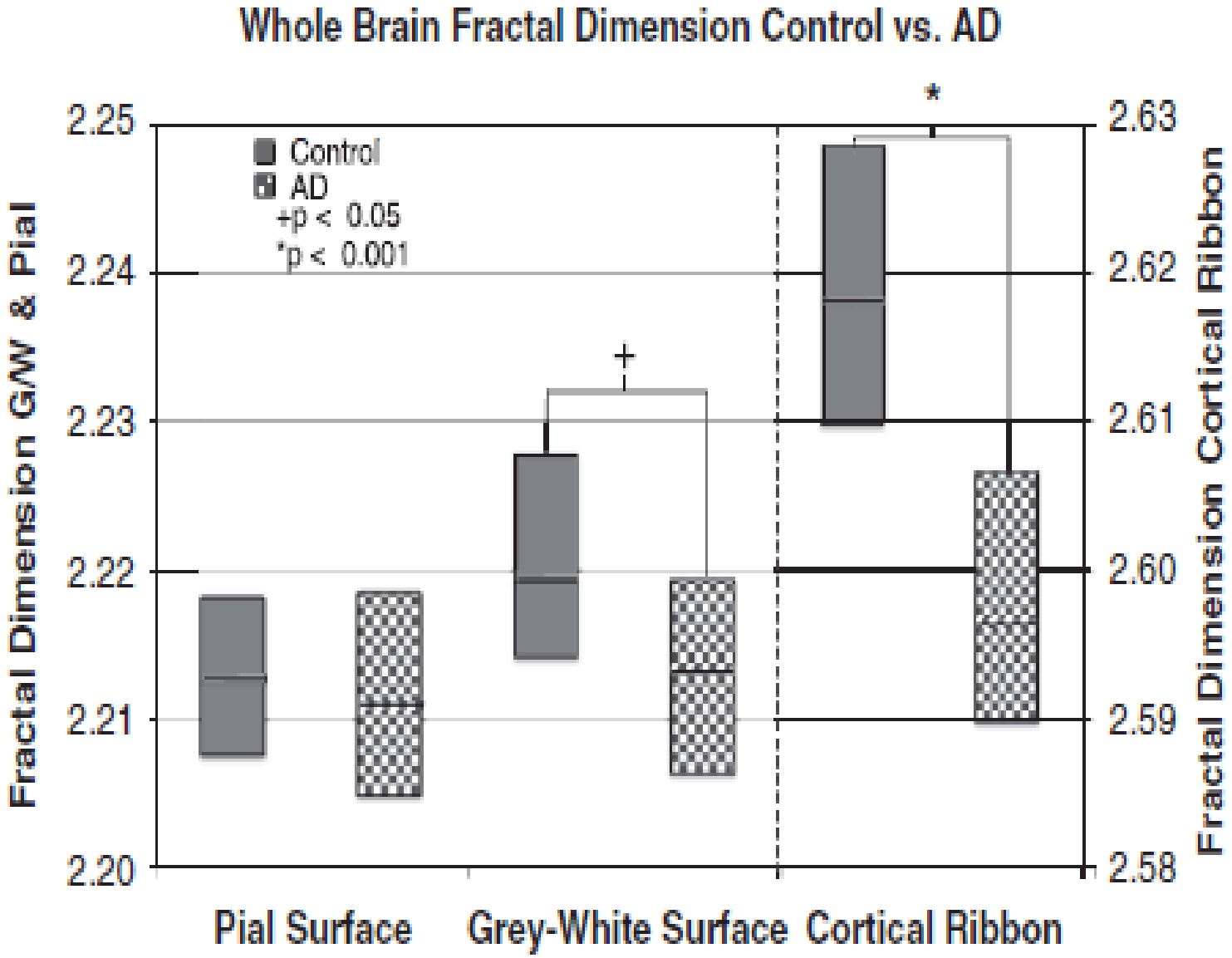

ig. 4. Differences in fractal dimension between groups of normal subjects and patients vith mild Alzheimer's disease (AD) as measured on the pial surface, gray/white surface nd the cortical ribbon. The boxes show the median value as the thick black line, and

Pellionisz, A. The Principle of Recursive Genome Function. The Cerebellum (Springer), 7(3) 348-359,2008

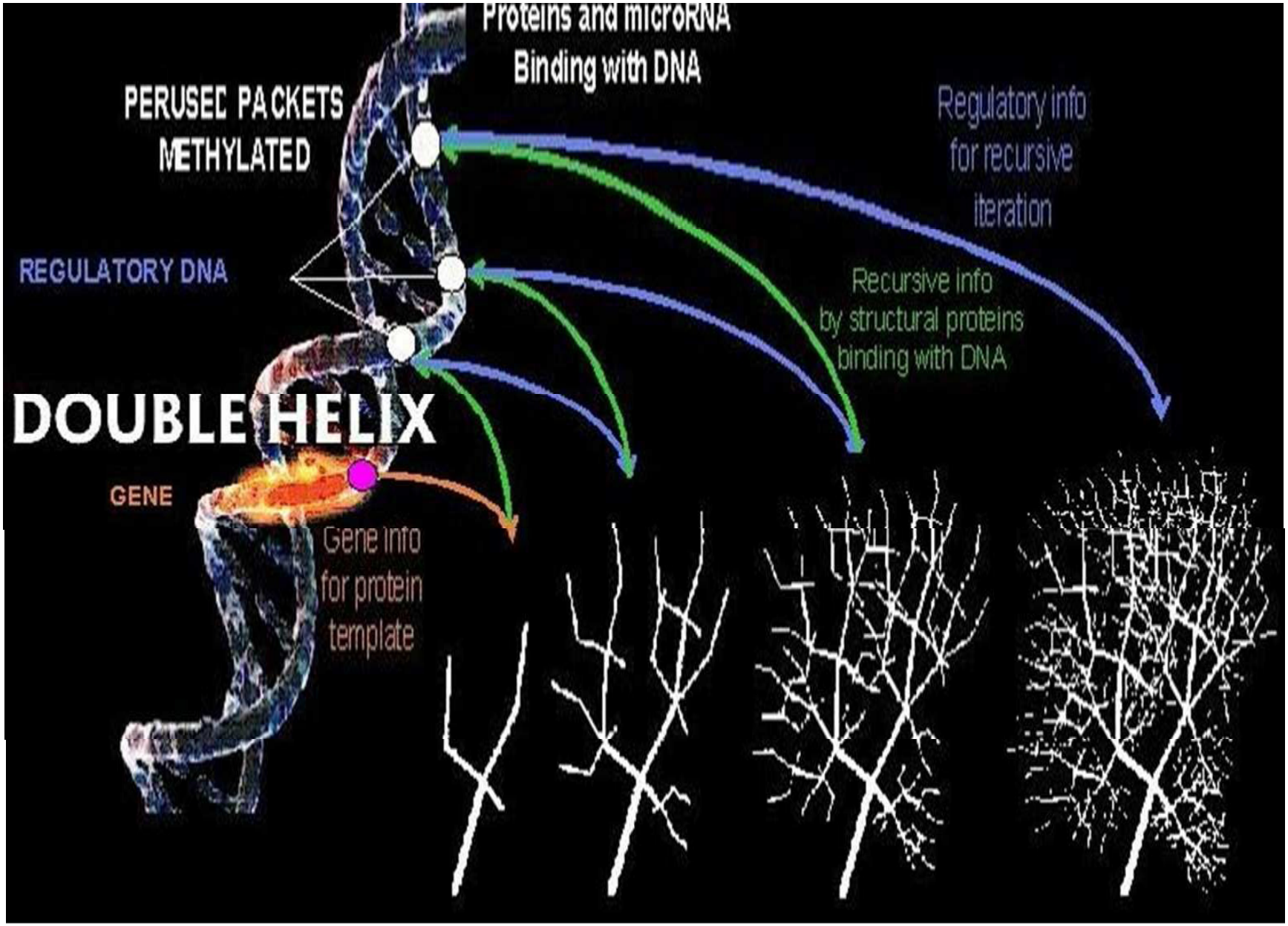

Considerations and Hypothesis

Morphogenesis of biostructures follows fractal principles

Fractal geometry is a design principle for living organisms and may be envisaged for interpreting how biological phenomena and shapes come about, while being well aware that the true reality may remain undisclosed!

Do genes contain fractal algorithms?
This appears much more interlocutory, because genes are DNA entities that codifyconstructive units or templates, while fractal algorithms represent mechanisms (iteration, self-organization, environmental constraints, etc.) which Nature may eventually adopt in order to assemble self-similar dynamic units into final biological shapes.
Genomic/functional analysis, such as the RNA-interference (RNAi) technique adapted to plants and mammalian cell cultures, has made it possible to screen systematically or genes controlling specific cell-biological processes, including those required to influence cytoskeletal organization, to generate distinct morphologies and, like *Hox* genes to act as architects which control the spatial structuring of the organism through its entire development.

Fractal model of the Purkinje neuron (of the guinea pig), which links for the first time the fractality of the genome with the fractality of neurons.The theoretical significance is that the fractality found in the DNA and organisms for a long time “apparently unrelated” was put into a “cause and effect” relationship by the Principle of Recursive Genome Function (Pellionisz 2008)